VOLUME 37 AUGUST 1959 NUMBER 8

Canadian Journal of Physics

Published by THE NATIONAL RESEARCH COUNCIL

OTTAWA CANADA

CANADIAN JOURNAL OF PHYSICS

Under the authority of the Chairman of the Committee of the Privy Council on Scientific and Industrial Research, the National Research Council issues THE CANADIAN JOURNAL OF PHYSICS and five other journals devoted to the publication, in English or French, of the results of original scientific research. Matters of general policy concerning these journals are the responsibility of a joint Editorial Board consisting of: members representing the National Research Council of Canada; the Editors of the Journals; and members representing the Royal Society of Canada and four other scientific societies.

Manuscripts for publication should be submitted to Dr. H. E. Duckworth, Editor, Canadian Journal of Physics, Hamilton College, McMaster University, Hamilton, Ontario.
For instructions on preparation of copy, see **NOTES TO CONTRIBUTORS** (back cover).

Proof, correspondence concerning proof, and orders for reprints should be sent to the Manager, Editorial Office (Research Journals), Division of Administration and Awards, National Research Council, Ottawa 2, Canada.

Subscriptions, renewals, requests for single or back numbers, and all remittances should be sent to Division of Administration and Awards, National Research Council, Ottawa 2, Canada. Remittances should be made payable to the Receiver General of Canada, credit National Research Council.

The journals published, frequency of publication, and prices are:

Canadian Journal of Biochemistry and Physiology	Monthly	$9.00 a year
Canadian Journal of Botany	Bimonthly	$6.00 a year
Canadian Journal of Chemistry	Monthly	$12.00 a year
Canadian Journal of Microbiology	Bimonthly	$6.00 a year
Canadian Journal of Physics	Monthly	$9.00 a year
Canadian Journal of Zoology	Bimonthly	$5.00 a year

The price of regular single numbers of all journals is $2.00.

Canadian Journal of Physics

Issued by THE NATIONAL RESEARCH COUNCIL OF CANADA

VOLUME 37 AUGUST 1959 NUMBER 8

COMPARISONS BETWEEN FREE ENERGIES OF ACTIVATION FOR GRAIN GROWTH, GRAIN-BOUNDARY SELF-DIFFUSION, AND LIQUID SELF-DIFFUSION[1]

E. L. HOLMES AND W. C. WINEGARD

ABSTRACT

A comparison is made between the free energies of activation for boundary migration during normal grain growth, grain-boundary self-diffusion, and liquid self-diffusion. The equality of these, within the accuracy of experiment and analysis, supports the assumption of identical elementary processes in the three cases. A detailed discussion is given regarding the various constants used in the equations from which the free energies of activation of the above-mentioned processes are derived.

INTRODUCTION

The near equality between the values obtained for the activation energies and free energies of activation for grain growth in zone-refined tin and lead and those for liquid self-diffusion has recently been noted by Holmes and Winegard (1959), who suggested that the elemental process may be the same in both cases. A comparison of the experimental results for normal grain growth with the theory of Cole, Feltham, and Gilliam (1954) indicated that over the temperature range investigated, the mechanism of boundary migration during normal grain growth involves a single-atom process. Aust and Rutter (1959) have made similar observations in their work on single-boundary migration in zone-refined lead. Holmes and Winegard (1959), by applying the theory of the kinetics of solidification as given by Jackson and Chalmers (1956), have further suggested that the energy barrier to be overcome in transferring an atom from the solid to the liquid during melting is comparable to the activation energy for grain growth in high-purity zone-refined materials. It has also been suggested by Beck *et al.* (1950) and Turnbull (1951) that the elementary process for grain-boundary migration is closely related to the elementary process in grain-boundary self-diffusion so that the free energies of activation for the two processes should be equal.

In this paper, values of the free energies of activation for grain-boundary self-diffusion, liquid self-diffusion, and, where possible, boundary migration during normal grain growth for various metals have been derived for purposes of comparison.

[1]Manuscript received March 13, 1959.
Contribution from the Department of Metallurgical Engineering, University of Toronto, Toronto, Ontario.

FREE ENERGIES OF ACTIVATION FOR LIQUID SELF-DIFFUSION AND GRAIN-BOUNDARY SELF-DIFFUSION

Values of the free energy of activation for self-diffusion in the liquid close to the freezing temperature are shown in Table I. The method of Mackenzie

TABLE I

Calculated free energies of activation at the melting temperature, using jump distance as 2 Å and boundary width as 5 Å

		Liquid self-diffusion kcal/g-atom		
Metal	Grain-boundary self-diffusion, kcal/g-atom	Calculated from Mackenzie and Hillig diffusion coefficients	Calculated from experimental data	Grain growth in zone-refined metals, kcal/g-atom
Lead	6.6 (Okkerse 1954)	4.8	4.4 (Rothman and Hall 1956)	6.2 (Bolling and Winegard 1958)
Tin		3.4	3.3 (Careri and Paoletti 1955)	3.2 (Holmes and Winegard 1959)
Silver	12.7 (Hoffman and Turnbull 1951)	9.1	10.3 (Ling Yang *et al.* 1958)	
Zinc	6.8 (Wadja 1954)	5.3		
Cadmium	4.4 (Wadja *et al.* 1955)	4.7		

and Hillig (1958) was used to obtain a liquid self-diffusion coefficient at the freezing temperature from which the appropriate free energy of activation was calculated using the expression:

$$D = \frac{\lambda^2}{6}\frac{kT}{h}\exp\left(-\frac{\Delta F_A}{RT}\right) \tag{1}$$

where λ is the jump distance, taken as 2 Å. This assumes that self-diffusion in the liquid is a near equilibrium process to which transition state theory may properly be applied. The form of equation (1) also assumes the simplest general case of six equivalent directions for the migration of each atom as discussed by LeClaire (1949). The free energy of activation for liquid self-diffusion was also calculated from experimental data where available, as indicated in Table I.

Also listed in Table I are values of the free energy of activation for grain-boundary self-diffusion derived by applying transition state theory to available experimental data in exactly the same manner as previously indicated, and following Hoffman and Turnbull (1951) and Wadja *et al.* (1955), assuming a boundary width of 5 Å.

FREE ENERGIES OF ACTIVATION FOR NORMAL GRAIN GROWTH IN ZONE-REFINED METALS

Turnbull (1951) has developed an equation for grain-boundary migration using the formalism of absolute reaction rate theory, viz.

$$G = e\left(\frac{kT}{h}\right)\lambda\frac{K\sigma V}{rRT}\exp\left(\frac{\Delta S_A}{R}\right)\exp\left(-\frac{Q_G}{RT}\right) \tag{2}$$

where G is the rate of grain-boundary migration;

$(kT)/h$ = the frequency factor;
λ = interatomic distance in the boundary;
K = a constant depending on grain shape;
σ = specific grain-boundary free energy;
r = the boundary radius of curvature;
V = the gram-atomic volume of the metal;
ΔS_A = the entropy of activation per gram atom;
and Q_G = the measured activation energy per gram atom.

The driving force for migration was assumed to be the reduction of total surface free energy; and if the other terms are treated as constants, the equation may be written as

$$G = \frac{G_0}{r}\exp\left(-\frac{Q_G}{RT}\right). \tag{3}$$

From this, the equation of grain growth, viz.

$$D = (Kt)^n, \tag{4}$$

is derived where D = grain diameter, t = time, and $K = K_0\exp(-Q/RT)$ such that $K_0 = aG_0$ and $Q = Q_G$ where a is a constant depending upon the nature of grain growth. By proper choice of constants in equation (2), the entropy of activation, and thus the free energy of activation per gram atom, may be obtained from

$$\Delta F_A = Q_G - T\Delta S_A - RT. \tag{5}$$

In the work of Bolling and Winegard (1958) on grain growth in zone-refined lead, the following values were chosen for the constants: $e = 2.72$, $k = 1.38\times10^{-16}$ ergs/° C, $h = 6.624\times10^{-27}$ ergs/sec, $K = 1$, $\sigma = 200$ ergs/cm², $V = 18.2$ cm³/g-atom, $\lambda = 2\times10^{-8}$ cm, and $a = 1$. The free energy of activation for grain growth in zone-refined tin near the melting temperature was calculated by Holmes and Winegard (1959) using the same constants, with the exception that for tin $V = 16.2$ cm³/g-atom and σ was taken as 100 ergs/cm² as estimated by Aust and Chalmers. These calculated values of free energy of activation for grain growth in zone-refined metals are also listed in Table I.

DISCUSSION

It is evident from Table I that an equality, within the limits of experiment and analysis, exists between the derived free energy of activation for liquid self-diffusion near the freezing temperature and for grain-boundary self-diffusion and grain growth near the melting temperature. This might be regarded as indicating that the elemental process may be similar in all three cases.

It is felt, however, that a critical discussion is required concerning the

choice of constants involved and the assumptions made in deriving the free energies of activation.

The following discussion is thus concerned with the constants used in equations (1) and (2).

(*a*) *Jump Distance*

Following Burke and Turnbull (1952) a somewhat arbitrary jump distance of 2 Å was chosen both for the boundary region and in the liquid state for the values listed in Table I.

With regard to the liquid state, there appear at present to be two possibilities:

(i) The jump distance is equal to the distance of the first maximum of the radial distribution function as given by X-ray measurements. If this is possible then it would appear that the calculated entropy of activation for liquid self-diffusion would have a negative value in many instances. This may mean that before a jump could occur, the disordered liquid would have to become ordered by assembling its free volume into a discrete hole of molecular dimensions, as suggested by Nachtrieb (1957). Only then would a single atom jump an interatomic distance in the vicinity of its stationary neighbors.

(ii) The entropy of activation is zero so that if the transition state theory applies the jump distance must be less than considered above. In this case, diffusion is not accomplished by isolated jumps of single atoms, but by the co-operative readjustment of many atoms. These possibilities have been discussed by Nachtrieb (1957).

The arbitrary value chosen, viz. 2 Å, is somewhat between the two extremes.

(*b*) *Boundary Width*

The value derived for the free energy of activation for grain-boundary self-diffusion depends very much on the choice of boundary width. This is discussed in some detail by McLean (1957), who concludes that for ordinary high-angle boundaries a choice of three atomic diameters is reasonable. If this value is chosen rather than 5 Å, then the calculated values of the free energy of activation for boundary self-diffusion would be increased somewhat, as seen in Table II.

(*c*) *The Constant K*

This constant depends on grain-boundary shape and, according to Burke and Turnbull (1952), should be of the order of 1 to 3. Feltham (1957) suggests that this constant should be 1 for a cylinder, 2 for a sphere, and concludes that the "best" value is 3/2, whereas Bolling and Winegard (1958) chose, arbitrarily, the lowest value, unity. Using the factor 3/2 for K, and assuming the other constants as before, the free energies of activation for grain growth in tin and lead near their melting temperatures are 6.9 kcal/g-atom and 3.7 kcal/g-atom, respectively, rather than 6.2 and 3.2 kcal/g-atom obtained when K is assumed to be unity.

(*d*) *The Specific Grain-Boundary Free Energy,* σ *ergs* cm^{-2}

The values of 200 ergs cm^{-2} for lead and 100 ergs cm^{-2} for tin, as estimated by Aust and Chalmers (1950, 1951), were chosen for calculating the values

TABLE II

(*a*) Liquid self-diffusion close to freezing temperature

Metal	Free energy of activation ΔF_A, kcal/g-atom	Entropy of activation ΔS_A, e.u.	Jump distance used, Å
Lead	5.70	−3.92	3.4
	3.25	0	1.272
Tin	4.25	−2.5	3.2
	3.00	0	1.716
Silver	5.7	0	0.78
	10.3	−3.75	2.0

(*b*) Grain growth close to melting temperature

Metal	Free energy of activation ΔF_A, kcal/g-atom	Entropy of activation ΔS_A e.u., cal/g-atom ° K	Values of constants, etc. used, i.e. K, λ, σ, 'a' taken as unity
Lead	4.60	1.50	$K = 1$, $\lambda = 1.272$ Å, $\sigma = 66$ ergs/cm²
	5.76	−0.433	$K = 1$, $\lambda = 3.4$, $\sigma = 66$
	7.08	−2.66	$K = 1$, $\lambda = 3.4$, $\sigma = 200$
	6.39	−1.50	$K = 3/2$, $\lambda = 1.272$, $\sigma = 200$
	7.56	−3.45	$K = 3/2$, $\lambda = 3.4$, $\sigma = 200$
	5.07	0.61	$K = 3/2$, $\lambda = 1.272$, $\sigma = 66$
	6.25	−1.25	$K = 3/2$, $\lambda = 3.4$, $\sigma = 66$
	6.70	−2.06	$K = 3/2$, $\lambda = 3.4$, $\sigma = 100$
Tin	3.15	3.68	$K = 1$, $\lambda = 1.716$ Å, $\sigma = 100$ ergs/cm²
	3.25	3.51	$K = 1$, $\lambda = 1.716$, $\sigma = 109$
	3.78	2.43	$K = 1$, $\lambda = 3.2$, $\sigma = 100$
	3.87	2.26	$K = 1$, $\lambda = 3.2$, $\sigma = 109$
	3.56	2.87	$K = 3/2$, $\lambda = 1.716$, $\sigma = 100$
	3.65	2.70	$K = 3/2$, $\lambda = 1.716$, $\sigma = 109$
	4.19	1.62	$K = 3/2$, $\lambda = 3.2$, $\sigma = 100$
	4.28	1.43	$K = 3/2$, $\lambda = 3.2$, $\sigma = 109$
	4.55	0.87	$K = 2$, $\lambda = 3.2$, $\sigma = 109$
	5.00	0.00	$K = 3$, $\lambda = 3.2$, $\sigma = 109$

(*c*) Grain-boundary self-diffusion in lead and silver close to melting temperature

Metal	Free energy of activation, kcal/g-atom	Jump distance, Å	Boundary width, Å
Lead	5.56	1.272	5.0
	9.10	3.4	5.0
	6.60	2.0	5.0
	4.66	1.272	2.0
	5.80	3.4	2.0
	7.50	2.0	10.0
Silver	8.1	0.78	5.0
	12.70	2.0	5.0
	14.1	2.0	8.7

shown in Table I. The assumption has been made that these values are constant over the temperature range investigated. Any variation with temperature of these values will mean that the entropy of activation for grain growth is also a function of temperature.

If a high-angle boundary may be regarded as a supercooled layer a few atoms thick, then the grain-boundary free energy may be expressed as the sum of the excess free energy of the supercooled layer over the solid, plus

twice the liquid–solid interfacial free energy. This model, as discussed by McLean (1957), requires an assumption regarding the effective width of the boundary. One might assume, however, that near the melting temperature the values 66 and 109 ergs cm^{-2}, viz. twice the solid–liquid interfacial free energy as given by Turnbull (1950) for lead and tin, respectively, might represent the specific boundary free energy. The consequences of this assumption are made evident in Table II.

(*e*) *The Constant "a"*

The formal theory of recrystallization kinetics, as discussed by Burke and Turnbull (1952), describes the process of isothermal recrystallization in terms of the parameters $\dot{N}$, the nucleation frequency, and G, the linear rate of growth. Burke and Turnbull (1952) point out that there is good evidence that the kinetics of normal grain growth after completion of recrystallization are controlled in large part by a parameter G that is closely related to the G values measured in primary recrystallization. To account for the fact that the G in normal grain growth cannot have the same formal relation to atomic mobility as G in recrystallization, the geometric factor 'a' is introduced. This factor is discussed by Burke and Turnbull (1952), who conclude that in general its value is less than unity. The value used in the calculations of the free energies of activation in this paper was arbitrarily chosen as unity.

In view of the above considerations, it is interesting to see just how the choice of jump distance, boundary width, and choice of constants used affect the calculated values of the free energies of activation.

Table II(*a*) shows possible values for the free energies and entropies of activation for liquid self-diffusion in lead, tin, and silver. Table II(*b*) lists both the free energies and entropies of activation for grain growth in zone-refined lead and tin close to their respective melting temperatures, and Table II(*c*) represents grain-boundary self-diffusion in lead, using the experimental data of Okkerse (1954), and silver, using the results of Hoffman and Turnbull (1951).

From the calculations in Table II(*c*), it is evident that, if the boundary region is regarded as being a definite region 5 Å in width and that within this region there exist six equivalent directions for the migration of each atom, then near the melting temperature a near equality exists between the calculated free energies of activation for grain growth, grain-boundary self-diffusion, and liquid self-diffusion, if we assume that a similar jump distance applies in all cases.

TEMPERATURE DEPENDENCE

It might be argued that the comparisons made in Tables I and II are valid only near the melting temperature. In the case of lead, tin, and silver, it is possible to make comparisons over a range of temperature.

Table III indicates that the temperature variations of the free energy of activation with regard to grain growth and liquid self-diffusion extrapolated to below the freezing temperature in both lead and tin are similar in nature.

TABLE III

Comparison between free energies of activation ΔF_A over a range of temperature, using a jump distance of 2 Å and boundary width of 5 Å

Metal	Temperature, °K	ΔF_A for grain-boundary self-diffusion, kcal/g-atom	ΔF_A for liquid self-diffusion, kcal/g-atom	ΔF_A for grain growth, kcal/g-atom
Lead	600	6.6	4.4	6.2
	550	7.3	4.4	6.2
	500	8.0	4.5	6.3
	400	8.6	4.5	6.3
Tin	500	—	3.3	3.2
	460	—	3.4	3.4
	440	—	3.4	3.6
Silver	1233	12.7	10.3	—
	1000	14.4	9.9	—
	900	15.1	9.8	—

However, it would appear that the free energies of activation for grain-boundary self-diffusion increase more rapidly as the temperature is decreased than is found to be the case for both grain growth and liquid self-diffusion. However, the measurements of grain-boundary self-diffusion were undertaken on relatively impure materials and so this difference in the temperature dependence of the free energy of activation for grain-boundary self-diffusion may be due to an increasing effect of the impurities in the boundary as the temperature is lowered. A critical assessment of impurity effects must be delayed until the conclusion of experiments now in progress concerning the effects of specific impurities on grain growth in zone-refined metals.

SUMMARY AND CONCLUSIONS

Investigations of normal grain growth in zone-refined lead and tin have indicated an equality between the values derived for the free energies of activation over a range of temperatures for grain-boundary migration and liquid self-diffusion extrapolated to below the freezing temperature.

Values of the free energy of activation for grain-boundary self-diffusion have been calculated for several metals, and a near equality has been found between these values close to the melting temperature and those calculated for liquid self-diffusion provided that the various assumptions made are not unreasonable. A difference in the variation of these free energies of activation with temperature was noted which may be due to the fact that the grain-boundary diffusion data was obtained using relatively impure materials. It is hoped that this will stimulate further work on self-diffusion in liquid metals and an investigation of grain-boundary self-diffusion in high-purity zone-refined materials. Despite the fact that the problem of the proper choice of constants, jump distances, grain-boundary thickness, etc., is a difficult one, the above results suggest that the activated state for the process whereby atoms move in liquid self-diffusion is the same as in the case of movement of

atoms within the grain-boundary region. This suggestion appears reasonable in view of our present state of knowledge regarding the structure of high-angle boundaries.

ACKNOWLEDGMENTS

The authors are grateful to the Defence Research Board of Canada (Grant No. 9535-01) for financial support. One of the authors, E. L. H., received an International Nickel Company Fellowship during the course of some of this work. The staff and graduate students of the Department of Metallurgical Engineering of the University of Toronto are to be thanked for their interest and stimulating discussions. The continued support and encouragement of Dr. L. M. Pidgeon is also gratefully acknowledged.

REFERENCES

AUST, K. T. and CHALMERS, B. 1950. Proc. Roy. Soc. A, **201**, 210.
——— 1951. Proc. Roy. Soc. A, **204**, 359.
AUST, K. T. and RUTTER, J. W. 1959. To be published.
BECK, P. A. *et al.* 1950. J. Appl. Phys. **21**, 420.
BOLLING, G. F. and WINEGARD, W. C. 1958. Acta Met. **6**, 283.
BURKE, J. E. and TURNBULL, D. 1952. Prog. in Metal Phys. **3**, 220.
CARERI, G. and PAOLETTI, A. 1955. Nuovo cimento, **2** (10), 574.
COLE, D. G., FELTHAM, P., and GILLIAM, E. 1954. Proc. Phys. Soc. B, **67**, 131.
FELTHAM, P. 1957. Acta Met. **5**, 97.
HOFFMAN, R. E. and TURNBULL, D. 1951. J. Appl. Phys. **22**, 634.
HOLMES, E. L. and WINEGARD, W. C. 1959. Acta Met. (to be published).
——— 1959. Can. J. Phys. **37**, 496.
JACKSON, K. A. and CHALMERS, B. 1956. Can. J. Phys. **34**, 473.
LECLAIRE, A. D. 1949. Prog. in Metal Phys. **1**, 334.
LING, Y., SATOSHI, K., and DERGE, G. 1958. Trans. Am. Inst. Mining Met. Engrs. 212.
MACKENZIE, J. D. and HILLIG, W. B. 1958. J. Chem. Phys. **28**, 1259.
MCLEAN, D. 1957. Grain boundaries in metals (Oxford University Press), p. 73.
NACHTRIEB, N. H. 1958. Liquid metals and solidification (Am. Soc. Metals), p. 49.
OKKERSE, B. 1954. Acta Met. **2**, 551.
ROTHMAN, S. J. and HALL, L. D. 1956. Trans. Am. Inst. Mining Met. Engrs. **206**, 199.
TURNBULL, D. 1951. Trans. Am. Inst. Mining Met. Engrs. **191**, 661.
TURNBULL, D. 1950. J. Chem. Phys. **18**, 769.
WADJA, E. S. *et al.* 1955. Acta Met. **3**, 39.
WADJA, E. S. 1954. Acta Met. **2**, 184.

EFFECTIVE AND THERMAL NEUTRON CAPTURE CROSS SECTION AND RESONANCE CAPTURE INTEGRAL OF Pr-143[1]

J. C. Roy and L. P. Roy

ABSTRACT

The effective neutron capture cross section, $\hat{\sigma}$; the 2200 meters/sec neutron capture cross section, σ_0, and the resonance capture integral, RI, of Pr-143 have been measured by an activation method. The values are: $\hat{\sigma} = 93 \pm 10$, $\sigma_0 = 89 \pm 10$, and $RI = 190 \pm 25$ barns respectively. The neutron fluxes have been measured with cobalt monitors. All these values have been calculated according to the Westcott convention, which has been outlined insofar as it can be applied to activation work.

INTRODUCTION

In order to obtain quantitative understanding of the changes in reactivity which occur during the irradiation of fuel in a nuclear reactor, a knowledge of the neutron capture cross sections of the fission products is necessary. At present, the cross sections of the more important fission products are known, but there are some fission products which may be significant poisons for which there is no information. Praseodymium-143 is in this class. It is reasonably long-lived, 13.6-day half life, and it is formed in high yield in fission, 6% in U^{235} fission. Furthermore, a knowledge of the neutron capture cross sections of the fission products is necessary for precise determination of fission product yields. It is therefore of interest to measure the neutron capture cross section of Pr^{143}.

Preliminary results of this work, reported in a recent review paper on cross sections of certain fission products by Eastwood *et al.* (1958), lead to a value of 124 barns for the effective cross section of Pr^{143}. Since then the two components of the effective capture cross section have been measured: that due to the Maxwellian component of the neutron flux, i.e. the thermal cross section, and that due to the epithermal component, the so-called resonance capture integral. Also the experiments reported here have led to an effective cross section which is lower than that reported earlier by about 30 barns; this change in the preliminary value is due to a reassessment of the efficiency of the counter used in the earlier experiments.

EXPERIMENTAL

(*a*) *Description of the Activation Method Used in the Measurement*

The capture cross sections of Pr^{143} were determined by an activation method involving the measurement of the 17.3-minute Pr^{144} formed by the (n,γ) reaction on Pr^{143}. The nuclear reactions leading to the formation of Pr^{143} and Pr^{144} upon irradiation of Ce^{142} are given in Fig. 1. It is seen that Pr^{144} can be

[1]Manuscript received May 4, 1959.
Contribution from the Chemistry and Metallurgy Division, Atomic Energy of Canada Limited, Chalk River, Ontario.
Issued as A.E.C.L. No. 823.

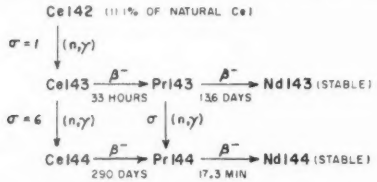

FIG. 1. Formation of nuclides of mass 143 and 144 by neutron irradiation of Ce-142.

formed by two separate routes. A relatively short irradiation of a large amount of cerium oxide was made, and the Ce^{143} so formed was allowed to decay out of the reactor for 10 to 15 days. Separate experiments, made according to the methods described in Sections (*b*) and (*c*), showed that no Pr^{144} was present in the material at that time. Thus the route

$$Ce^{142} \xrightarrow{(n,\gamma)} Ce^{143} \xrightarrow{(n,\gamma)} Ce^{144} \xrightarrow{\beta^-} Pr^{144}$$

was unimportant for the formation of Pr^{144}. This result was not unexpected, since the neutron cross section of Ce^{143} is only 6 barns (Roy and Yaffe 1956).

Following the out-of-reactor period (during which more than 99% of the Ce^{143} formed in the first irradiation had decayed to Pr^{143}) aliquots of the Pr^{143}–Ce mixture were reirradiated for 10 to 30 minutes, and the product examined quickly for Pr^{144}. This two-stage irradiation, without an intervening chemical separation, clearly allows a quantitative distinction to be made between the two possible routes for the formation of Pr^{144} from Ce^{142}. Formation of Pr^{144} must come from neutron capture in Pr^{143}, and not from the alternate route involving neutron capture in Ce^{143}.

In these experiments the measurement of the activity of Pr^{144} rests on the fact that the 3.0-Mev beta rays of Pr^{144} can be counted in the presence of the intense Pr^{143} activity by absorbing the 0.92-Mev beta rays of the latter in aluminum. The amount of Pr^{144} formed was obtained from its beta disintegration rate and, after the Pr^{144} had decayed, the amount of Pr^{143} used in the experiment was also obtained from its beta disintegration rate. This method has the advantage that the amounts of Pr^{144} and Pr^{143} were obtained from the same source so that the determination of a chemical yield is not necessary.

(*b*) *Irradiation and Chemical Purification*

Ten aliquots of the Pr^{143}–Ce mixture were irradiated in an empty fuel rod position in the NRX reactor. The irradiations were done in groups of two; for each group, the first sample was irradiated in an iron capsule; the second sample was irradiated in an iron capsule lined with 0.076 cm of cadmium. For each group of irradiations the power of the reactor was constant. Immediately following each irradiation, cobalt wires, 0.0127 cm in diameter, 1 cm in length, and 1.151 mg in weight (Jervis 1957), were irradiated in iron and cadmium-lined iron capsules from 2 to 5 minutes in order to measure both the thermal and epithermal fluxes.

After the short irradiations a fast separation of Pr from Ce was made by the

iodate method. The reirradiated cerium oxide was dissolved in boiling concentrated sulphuric acid to which 2 to 3 ml 30% hydrogen peroxide was added. After addition of Pr carrier, both Pr and Ce were precipitated with ammonia and the precipitate was dissolved in nitric acid. The cerium was oxidized to the tetravalent state by the addition of solid potassium bromate and was precipitated as the iodate. The precipitate was centrifuged and discarded. The supernatant, containing the Pr, was neutralized with 12 *N* NaOH. In the first few experiments the praseodymium precipitate was dissolved and two more cerium scavengings were made, but it was found that the additional cerium scavengings did not improve appreciably the radiochemical purity of $Pr(OH)_3$ precipitate. Therefore in the subsequent experiments, these extra scavengings were omitted to save time. The final $Pr(OH)_3$ precipitate was deposited onto a "Millipore" filter paper. The filter paper was transferred on an aluminum disk and dried. The $Pr(OH)_3$ was now ready for counting.

(*c*) *Counting of the Samples and Absolute Rate Determinations*

The disk on which the $Pr(OH)_3$ precipitate was mounted was covered with 400 mg/cm^2 of aluminum. This thickness will absorb all the 0.92-Mev beta rays of Pr^{143}. The source was counted with an end window methane flow counter. The activities of the sources were measured until the Pr^{144} had decayed completely and also several hours later to estimate the contribution of a long-lived activity. The efficiency of the counter under that arrangement was determined by counting aliquots of a source of Pr^{144}, separated from the fission product Ce^{144}, in a 4π beta proportional counter and in the flow counter under the conditions just described. It was found to be 5.8%.

From the efficiency of the counter, and the time elapsed between the end of the irradiation and the beginning of the count, the absolute disintegration rate of Pr^{144} was obtained. A half life of 17.3 minutes for Pr^{144} was assumed (Peppard *et al.* 1957).

After the 17.3-minute Pr^{144} had decayed, the $Pr(OH)_3$ was dissolved in nitric acid and the solution was made up to a known volume. Aliquots of the solution were evaporated on to gold-coated VYNS films of about 20 μg/cm^2 for absolute beta disintegration rate in a 4π beta proportional counter. It was found necessary to cover the sources with an additional VYNS film coated with gold to get sufficient conductivity to avoid losses in the counting rate. Two sources were made up from each solution and their decay was followed for two half lives. The number of atoms of Pr^{143} in the (n,γ) reaction producing Pr^{144} was obtained from that determination by extrapolating the disintegration to the midtime of the irradiation using 13.6 days for the half life of Pr^{143} (Peppard *et al.* 1957).

(*d*) *Identification of* Pr^{144}

In all the determinations, the short-lived activities after subtraction of a residual activity had half lives ranging from 17.3 to 18.9 minutes. Figure 2 shows the decay curves of the activities for the group of experiments labelled E in Table II. A separate experiment was done to show that the short-lived activity was due to Pr^{144} and not to some other radioactive species carried

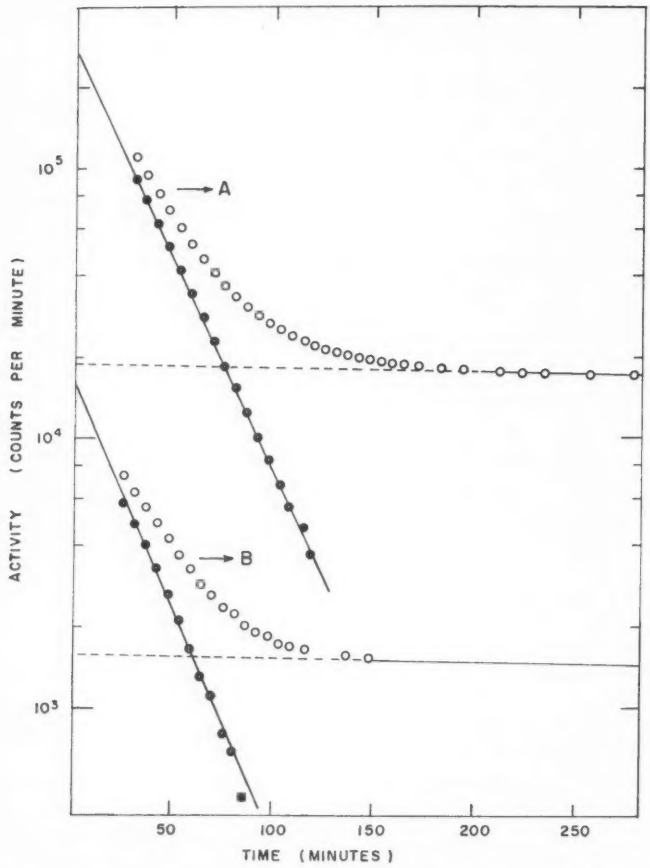

FIG. 2. Decay curves of Pr^{144} activities for the group of experiments labelled E in Table II; A, irradiation done without cadmium filter; B, irradiation done with cadmium filter. ○ gross activity; ● activity due to Pr-144; – – – residual activity.

down with the $Pr(OH)_3$ precipitate. A sample of cerium oxide, free from Pr^{143}, was irradiated for 1 hour in a high-flux position of the reactor. In such an irradiation the amount of Pr^{143} formed is much too low to lead to a detectable amount of Pr^{144} by a (n,γ) reaction. Praseodymium was separated and counted as described in Sections (*b*) and (*c*). No activities with half lives in the range of 10 minutes to a few hours were detected.

The residual activity in the $Pr(OH)_3$ precipitate found after the decay of Pr^{144} showed a half life of about 20 hours. It could be due to Pr^{142} formed by the $Pr^{141}(n,\gamma)Pr^{142}$ reaction; Pr^{142} has a 2.1-Mev beta ray and Pr^{141} would have been partly produced by the decay of Ce^{141} and it could have been present initially as an impurity in the cerium oxide.

(*e*) *Flux Measurements*

The gamma activities of cobalt were measured by placing the monitors inside a well-shaped hole of a NaI(Tl) crystal coupled to an RCA 5819 photomultiplier tube. The pulses above 0.66 Mev were registered in a single-channel analyzer. The spectrometer was calibrated with a Co^{60} source whose absolute activities were determined by 4π β- and γ-coincidence counting. The measured γ-activities have been corrected for the self-shielding effects arising from the absorption and the scattering of the neutrons in the monitor. For the monitor used in the experiments, Eastwood (1959) has found that the observed reaction rates without and with cadmium filters have to be multiplied by 1.04 and 1.62 respectively. These corrections will give the reaction rates that one normally would observe in using an infinitely thin cobalt wire. For the irradiations without cadmium filters, absorption and scattering of the neutrons are responsible for the correction in about the same amount; for those under cadmium filters, the large correction arises from the scattering resonance of Co^{59} for neutrons of 132 ev. The disintegration rates extrapolated to the end of the irradiation were obtained using a half life of 5.28 years for Co^{60} (Hughes and Schwartz 1958).

The precision of the measurements of the thermal and epithermal fluxes was 1 and 2% respectively.

(*f*) *Errors*

The combined uncertainties in obtaining the absolute disintegration rates of Pr^{144} and Pr^{143} are estimated to be about 10% for the irradiations without cadmium and about 15% for those done under cadmium filter. As they are the major source of errors, the final results are estimated to be precise within these limits, that is 10% for the capture cross sections and 15% for the resonance capture integral.

RESULTS

To obtain the flux from the cobalt monitor measurements and the capture cross sections of Pr^{143} the convention described by Westcott *et al.* (1958) was used. Eastwood *et al.* (1958) have already described and applied this convention to the measurement of neutron fluxes and cross sections by an activation method. In view of the novelty of the convention, however, it may be useful to repeat its main features and to give the equations applicable to the results found in activation work.

1. This convention is *based* on equating the measured reaction rate, R, per atom of capturing nuclide to the product of the effective cross section, $\hat{\sigma}$, and the reactor thermal neutron flux, nv_0, where n is the total neutron density in neutrons/cm^3 and v_0 is 2200 meters/sec. The term nv_0 is usually called conventional flux. Thus

$$R = \hat{\sigma}\, nv_0. \tag{1}$$

The units of R are atoms of product per unit time per atom of capturing nuclide. For convenience in activation experiments R can be given as

$$R = \frac{dN/dt}{N_0(1-e^{-\lambda t})} \tag{2}$$

where dN/dt is the disintegration rate of the product at the end of the irradiation, N_0 is the number of atoms of capturing nuclide, λ is the disintegration constant of the product, and t the time of irradiation.

2. In a well-moderated thermal neutron reactor, such as NRX, the neutron spectrum is *assumed* to consist of two components: the first a Maxwellian distribution with a characteristic temperature T °K without energy limits, the second a dE/E flux distribution (the epithermal region) subject to a suitable lower energy limit = μkt, but overlapping the Maxwellian component. The value of μkT is thought to be about 0.125 ev for heavy water moderators. In activation measurements, however, the dE/E distribution is cut off at 0.5 ev by the use of a cadmium filter. It is therefore more convenient to use the effective cadmium cutoff rather than μkT as the lower energy limit. This interpretation makes the resonance capture integral smaller by 2% for an absorber which follows the "$1/v$" law in the 0.125 to 0.5 ev region.

3. Subject to the assumptions of Section 2, the effective cross section is defined by the relation:

$$\hat{\sigma} = \sigma_0(g+rs) \tag{3}$$

where $\sigma_0 = \sigma_{2200}$, r is a measure of the relative density of the epithermal component of the neutron spectrum, and g and s are factors which depend on the departure of the cross section from the "$1/v$" law in the Maxwellian and dE/E components respectively.

4. The value of r is a characteristic of the reactor and in addition varies within the reactor. It is related to the cadmium ratio, R_{Cd}, by an equation to be given later. When the neutron spectrum is a pure Maxwellian r is 0. The values of g and s have been tabulated for the most important nuclides, over a range of neutron temperatures (Westcott 1958). However, these tables cannot be used in activation work because the neutron temperatures are not usually known. The additional assumption that $g = 1$ has to be made; fortunately this is the case for most substances including the important detector Co^{59}. To obtain s, without a measurement of the neutron temperature, a new factor, s_0, is introduced such that

$$s_0 = s\sqrt{\frac{T_0}{T}}. \tag{4}$$

The value of $s\sqrt{(T_0/T)}$ can be obtained from equation A1.2 in Westcott's report CRRP-785 (1958) which is:

$$s_0 = s\sqrt{\frac{T_0}{T}} = \sqrt{\frac{4}{\pi}}\left(\frac{RI}{\sigma_0} - \sqrt{\frac{4E_0}{E_{Cd}}}\right) \tag{5}$$

where RI is the resonance integral of the absorber, including the $1/v$ part, $E_0 = kT_0 = 0.025$ ev, and E_{Cd} is the cadmium cutoff energy taken to be 0.5 ev for 0.076 cm of cadmium.

Equation (3) can now be written

$$\hat{\sigma} = \sigma_0\left(1+r\sqrt{\frac{T}{T_0}}s_0\right). \tag{6}$$

Following the convention, $r\sqrt{(T/T_0)}$ is related to the cadmium ratio, R_{Cd}, and s_0 by equation 11*a* of Westcott *et al.* (1958), which for convenience can be given the form:

$$r\sqrt{\frac{T}{T_0}} = \frac{1}{R_{Cd}(s_0+1/K)-s_0}. \tag{7}$$

The cadmium ratio is the ratio of the reaction rate of the absorber without cadmium to the reaction rate with a cadmium filter. The factor K is a coefficient calculated from the variation of the cadmium cross section with neutron energy and the thickness of cadmium used in the irradiation. Values of K for thicknesses of cadmium in common use are tabulated by Westcott *et al.* (1958); for 0.076 cm of cadmium, the thickness used in these experiments, with an isotropic incidence of neutrons, $K = 2.2$.

From equations 1 to 7 and by reference to a standard (cobalt in these experiments) $\hat{\sigma}$, σ_0, and the resonance capture integral for any absorber can be measured by an activation method.

(*a*) *Westcott's Convention Applied to Flux Calculations*

In the application of the convention to the calculation of neutron fluxes from cobalt monitors the factor s_0 is evaluated from equation 5. From the measured cadmium ratio of cobalt for the irradiation position used and the values of s_0 and K, $r\sqrt{(T/T_0)}$ is obtained by application of equation 7. Then $\hat{\sigma}$ can be deduced for cobalt using equation 6. From this nv_0 follows from equation 1; R is the reaction rate without cadmium filter obtained from equation 2.

The conventional neutron fluxes obtained in this way and the data necessary for their calculation have been assembled in Table I. The value of σ_0 for Co^{59}

TABLE I

Conventional neutron fluxes measured with cobalt monitors

Experiment			Duration of irradiation, seconds	dN/dt,* d.p.s.	dN/dt,† d.p.s.	N,‡	R,§ sec^{-1}	R_{Cd}, Co-59	s_0	$r\sqrt{(T/T_0)}$	$\hat{\sigma}$, barns	nv_0, n/cm²-sec
A	1	No Cd	120	13,390	13,930	1.176×10^{18}	2.37×10^{-9}	19.4	1.80	0.0238	38.2	6.20×10^{13}
	2	Cd	120	442	717	"	1.22×10^{-10}					
B	3	No Cd	120	13,040	13,560	"	2.31×10^{-9}	18.9	1.80	0.0245	38.2	6.05×10^{13}
	4	Cd	300	1,100	1,785	"	1.22×10^{-10}					
C	5	No Cd	300	33,250	34,580	"	2.36×10^{-9}	17.6	1.80	0.0264	38.3	6.16×10^{13}
	6	Cd	300	1,210	1,960	"	1.34×10^{-10}					
D	7	No Cd	120	13,170	13,700	"	2.33×10^{-9}	19.4	1.80	0.0238	38.2	6.10×10^{13}
	8	Cd	300	1,090	1,760	"	1.20×10^{-10}					
E	9	No Cd	120	12,880	13,400	"	2.28×10^{-9}	19.5	1.80	0.0237	38.2	5.97×10^{13}
	10	Cd	300	1,060	1,720	"	1.17×10^{-10}					

*Disintegration rate of Co^{60} at the end of the irradiation, uncorrected for self-shielding.
†Disintegration rate of Co^{60} at the end of the irradiation, corrected for self-shielding.
‡Number of atoms of Co^{59} present during the irradiation.
§Rate of the $Co^{59}(n,\gamma)Co^{60}$ reaction.

is taken to be: $\sigma_0 = 36.68$ barns, the average of the two values in BNL-325, 2nd edition (Hughes and Schwartz 1958). The value of the resonance capture integral of Co^{59}, including the $1/v$ part, for an infinitely thin wire of cobalt is 75 ± 5 barns (Johnston *et al.* 1959; Eastwood 1959).

(*b*) *Capture Cross Sections and Resonance Integral of* Pr^{143}

The effective cross section of the reaction $Pr^{143}(n,\gamma)Pr^{144}$ is calculated from its observed reaction rate without cadmium filter and from the conventional flux using equation 1. The flux has already been measured; the reaction rate is calculated from equation 2.

The cadmium ratio for Pr^{143} has been measured in each group of experiments. Then the factor s_0 for Pr^{143} can be calculated from equation 7 where $r\sqrt{(T/T_0)}$, which is a constant of the reactor for the irradiation position used, has already been determined. The 2200 meters/sec cross section of Pr^{143} can now be calculated from the values of $\hat{\sigma}$, s_0, and $r\sqrt{(T/T_0)}$ by application of equation 6.

The neutrons in the dE/E flux distribution have equal flux per energy interval of $\ln E$ in a well-moderated thermal neutron reactor such as NRX so that the resonance capture integral, RI, can be defined as $\int_{0.5}^{\infty} \sigma_e(E) dE/E$ with the integral evaluated from $E_{Cd} = 0.5$ ev to fission energies. Following the convention the resonance capture integral was obtained from equation 5.

The values of $\hat{\sigma}$, σ_0, and RI for Pr^{143} and the data needed to obtain them have been compiled in Table II. The average of the five determinations, including

TABLE II

Capture cross section and resonance capture integral of Pr-143

Experiment Group	No.	Duration of irradiation, seconds	nv_0 (from Table I), n/cm²-sec	dN/dt,* d.p.s.	N†	R,‡ sec^{-1}	R_{Cd}, Pr-143	$\hat{\sigma}$, barns	s_0	σ_0, barns	RI, barns
A	1	600	6.20×10^{13}	19,250	9.56×10^{22}	6.09×10^{-9}	18.7	98.2	1.89	94.0	200
	2	600		671	6.24×10^{22}	3.26×10^{-10}					
B	3	1800	6.05×10^{13}	37,420	10.03×10^{22}	5.34×10^{-9}	16.3	88.3	2.18	83.8	200
	4	1800		471	2.06×10^{22}	3.27×10^{-10}					
C	5	1800	6.16×10^{13}	71,050	17.80×10^{22}	5.71×10^{-9}	18.5	92.7	1.69	88.7	173
	6	1800		4,480	20.80×10^{22}	3.08×10^{-10}					
D	7	1800	6.10×10^{13}	50,550	12.25×10^{22}	5.90×10^{-9}	20.9	96.7	1.63	93.1	176
	8	1800		2,230	11.31×10^{22}	2.82×10^{-10}					
E	9	1800	5.97×10^{13}	86,730	23.30×10^{22}	5.32×10^{-9}	17.1	89.1	2.13	84.8	198
	10	1800		4,535	20.83×10^{22}	3.11×10^{-10}					
							Mean	93.0		89.0	190

*Disintegration rate of Pr^{143} at the end of the irradiation.
†Number of atoms of Pr^{143} present during the irradiation.
‡Rate of $Pr^{143}(n,\gamma)Pr^{144}$ reaction.

the estimated errors as discussed in Section (*e*) of Experimental, gives values of $\hat{\sigma} = 93 \pm 10$, $\sigma_0 = 89 \pm 10$, and $RI = 190 \pm 25$ barns.

Note that, unlike the observed γ-activities of Co^{60}, the observed β-activities

of Pr^{144} have not been corrected for the self-shielding of the neutrons in the target material. It is assumed that no self-shielding corrections are necessary for the amounts of cerium oxide used in the measurements, because the thermal absorption cross section of cerium is only 0.73 barn and the total cross section is fairly constant at 4 barns from 1.0 ev to 1.0 Mev, with the exception of a small resonance at 140 kev (Hughes and Schwartz 1958).

REFERENCES

EASTWOOD, T. A. 1959. Private communication.

EASTWOOD, T. A., BAERG, A. P., BIGHAM, C. B., BROWN, F., CABELL, M. J. GRUMMITT, W. E., ROY, J. C., ROY, L. P., and SCHUMAN, R. P. 1958. Second International Conference on the Peaceful Uses of Atomic Energy, Geneva, paper P/203.

HUGHES, D. J. and SCHWARTZ, R. T. 1958. Brookhaven National Laboratory Report, BNL-325, 2nd edition.

JERVIS, R. E. 1957. Atomic Energy of Canada Limited, Report CRDC-730.

JOHNSTON, F. J., HALPERIN, J., and STOUGHTON, R. W. 1959. To be published.

PEPPARD, D. F., MASON, G. W., and MOLINE, S. W. 1957. J. Inorg. & Nuclear Chem. **5**, 141.

ROY, L. P. and YAFFE, L. 1956. Can. J. Chem. **34**, 238.

WESTCOTT, C. H. 1958. Atomic Energy of Canada Limited, Report CRRP-787.

WESTCOTT, C. H., WALKER, W. H., and ALEXANDER, T. K. 1958. Second International Conference on the Peaceful Uses of Atomic Energy, Geneva, paper P/202.

THE CUMULATIVE FISSION YIELDS OF LIGHT MASS FRAGMENTS IN THE THERMAL NEUTRON FISSION OF Pu^{239}[1]

H. R. Fickel[2] and R. H. Tomlinson

ABSTRACT

The relative cumulative yields of 19 light mass fragments of rubidium, strontium, yttrium, zirconium, molybdenum, and ruthenium formed in the thermal neutron fission of Pu^{239} have been determined with a mass spectrometer using the isotope dilution technique.

The yields of the fission product isotopes of these elements, together with the previously published relative yields of three krypton isotopes, have made possible the determination of the absolute yields of 22 light fragment mass chains.

INTRODUCTION

Published values for the absolute cumulative yields of the light mass fragments formed in the thermal neutron fisson of Pu^{239} consist of only a few radiochemically determined yields summarized by Katcoff (1958), the absolute yields of Sr^{88} and Sr^{90} reported by Krizhanskii and Murin (1958), and the yields of the krypton isotopes determined at the same time as the present work by Fritze *et al.* (1958) using a mass spectrometer.

The absolute yields of the strontium isotopes reported by Krizhanskii and Murin (1958) are based on the normalization of their relative yields to the 5.98% yield of Nd^{143} reported by Wiles *et al.* (1956). These values should therefore be renormalized to the more accurate value of 4.56% for the yield of Nd^{143} (Fickel and Tomlinson 1959).

The cumulative yields of 19 mass chains in the light mass fragments have been determined in the present work and compared with the previously reported values.

EXPERIMENTAL

Plutonium was irradiated in the NRX (Chalk River) reactor both as PuO_2 sealed in quartz tubes and Pu–Al alloy. The irradiation data are shown in Table I. Complete dissolution of the PuO_2 after irradiation was accomplished by conversion to the fluoride by alternate treatment with HF and HCl solutions during a period of several days.

The relative yields of the isotopes of rubidium, strontium, and yttrium were determined using the mass spectrometer with no prior chemical separations from the other fission products. However, carrier-free separation techniques were required in the analyses of zirconium, molybdenum, and ruthenium fission products.

In the case of zirconium, advantage was taken of its colloidal-forming tendency in neutral solution. The separation was accomplished by the dialysis

[1]Manuscript received May 19, 1959.
Contribution from Chemistry Department, McMaster University, Hamilton, Ontario.
[2]Holder of an International Nickel Company Limited Fellowship, 1958–1959. Holder of Canadian Industries Limited Fellowship, 1957–1958.

TABLE I

Irradiation data for plutonium samples

Sample	Weight, g	Chemical form	Irradiation time, days	Average neutron flux $\times 10^{13}$, n/cm² sec
1	0.01091	PuO_2	31.2	0.56*
2	0.01034	PuO_2	51.03	1.00*
3	0.01012	PuO_2	51.57	0.346
4	0.0758	13.9% Pu–Al alloy	23.53	0.194
5	0.1520	13.9% Pu–Al alloy	34	0.86
6	0.1566	13.9% Pu–Al alloy	30.0	0.311
7	0.10551	10% Pu–Al alloy	30	6.6*
8	0.10061	10% Pu–Al alloy	34	5.56
9	0.10361	10% Pu–Al alloy	25	7.00

*Only approximate, obtained from Reactor Operation Report.

of a neutral solution of the irradiated sample. As described by Schubert (1949), maximum efficiency was achieved at a pH greater than 5 from a solution completely free from such anions as F^-, $C_2O_4^=$, and $PO_4^{\equiv}$.

Excess acid was removed from the solution of the irradiated sample by repeated evaporations to dryness and dissolutions in water. The solution was dialyzed and the contents of the dialyzer was analyzed with the mass spectrometer. Whereas the separation from the other fission products was essentially complete by this method, only a partial separation from plutonium was obtained.

The molybdenum was separated by three extractions from an aqueous 6 *N* HCl solution using equal volumes of ethyl ether saturated with 6 *N* HCl. The ether extracts were combined and analyzed with the mass spectrometer.

Ruthenium was separated from the other elements in a glass apparatus by an oxidative distillation. A solution of 0.16 *N* $KMnO_4$ and 36 *N* H_2SO_4 was used to oxidize the ruthenium to the volatile ruthenium tetroxide which was collected in the distillate by reduction with a dilute solution of H_2O_2 and HNO_3.

Samples 3, 8, and 9 were used for obtaining absolute yield data. For samples 3 and 8 a small fraction ($< 1\%$) of the solution was analyzed with the mass spectrometer for the presence of contamination of the fission product elements by stable isotopes. Samples 8 and 9 were portions of the same piece of unirradiated plutonium–aluminum alloy; hence no preliminary contamination check was made for sample 9. This sample was dissolved directly in a mixture of the isotope diluents required for the analysis. The method of isotope dilution has been described previously by Petruska *et al.* (1955).

EXPERIMENTAL RESULTS

The relative yields of the isotopes of the elements strontium, zirconium, yttrium, molybdenum, and ruthenium are shown in Tables II to VI. The data given in Table II include measured mass spectrometric ratios of the strontium isotopes together with the ratios after contamination correction and the decay corrections for Sr^{89} and Sr^{90} have been made.

TABLE II

Relative yields of strontium isotopes in the thermal neutron fission of Pu^{239}

Sample	Time from end of irradiation, days	Isotope	Mass spectrometric ratio	Ratio corrected: For contamination	Ratio corrected: For decay
2	70.78	86	0.02667±0.00029	—	—
		88	0.871±0.018	0.648±0.013	0.644±0.013
		89	0.2212±0.0025	0.2212±0.0025	0.7846±0.0089*
		90	1.000	1.000	1.000†
8	57.0	86	—	—	—
		88	0.6590±0.0062	0.6590±0.0062	0.6550±0.0062
		89	—	—	—
		90	1.000	1.000	1.000†

*$t_{\frac{1}{2}}$ for Sr^{89} = 51.8 days (Fickel and Tomlinson unpublished).
†$t_{\frac{1}{2}}$ for Sr^{90} = 27.7 years (Wiles *et al.* 1955).

TABLE III

Relative yields of zirconium isotopes in the thermal neutron fission of Pu^{239}

Sample	Time from end of irradiation, days	Isotope	Mass spectrometric ratio	Ratio corrected: For contamination	Ratio corrected: For decay
1		90	3.361	—	—
	67.3	91	1.167±0.023	—	—
		92	1.907±0.020	0.789±0.020	0.789±0.020
		93	1.000	1.000	1.000
		94	2.261±0.024	1.125±0.024	1.125±0.024
	105.7	95	0.3545±0.0062	0.3545±0.0062	1.266±0.022*
		96	1.478±0.016		
5		90	0.1818	—	—
	428.4	91	0.692±0.013	0.656±0.013	0.656±0.013†
		92	0.852±0.021	0.791±0.021	0.791±0.021
		93	1.000	1.000	1.000
		94	1.193±0.015	1.131±0.015	1.131±0.015
	431	95	—	—	—
		96	1.322±0.018	1.312±0.018	1.312±0.018

*$t_{\frac{1}{2}}$ for Zr^{95} = 65.8 days (Fickel and Tomlinson unpublished data).
†$t_{\frac{1}{2}}$ for Y^{91} = 58 days (Kahn *et al.* 1955).

TABLE IV

Relative yields of yttrium isotopes in the thermal neutron fission of Pu^{239}

Sample	Isotope	Time from end of irradiation, days	Mass spectrometric ratio	Ratio corrected for decay
2	89	70.80	1.000	1.00
	91		0.6433±0.0098	1.44±0.02
2	89	98.4	1.000	1.00
	91		0.4156±0.0066	1.44±0.02

NOTE: $t_{\frac{1}{2}}$ for Sr^{89} = 51.8 days (Fickel and Tomlinson unpublished).
$t_{\frac{1}{2}}$ for Y^{91} = 58 days (Kahn *et al.* 1955).

TABLE V

Relative yields of molybdenum isotopes in the thermal neutron fission of Pu^{239}

Sample	Time from end of irradiation, days	Isotope	Mass spectrometric ratio	Ratio corrected: For contamination	Ratio corrected: For decay
3	417.73	95	0.790±0.022	0.695±0.022	0.711±0.022*
		96	1.008	—	—
		97	0.856±0.014	0.797±0.014	0.797±0.014
		98	0.968±0.018	0.824±0.018	0.824±0.018
		100	1.059	1.000	1.000
7	84	95	—	—	—
		96	0.3498	—	—
		97	0.994±0.017	0.794±0.017	0.794±0.017
		98	1.335±0.015	0.832±0.015	0.832±0.015
		100	1.204	1.000	1.000

*Assuming 65.8-day half-life for Zr^{95} and 35-day half-life for Nb^{95} (Engelkemeir *et al.* 1951; Cork *et al.* 1953).

TABLE VI

Relative fission yields of ruthenium isotopes in fission of Pu^{239}

Sample	Time from end of irradiation, days	Isotope	Mass spectrometric ratio	Ratio corrected for decay
6	668.0	101	1.000	1.000
½ of 4	664.1	102	1.013±0.014	1.013±0.014
		104	1.003±0.014	1.003±0.014
		106	0.215±0.075	0.773±0.027
9	92	103	0.1151±0.0019	0.9601±0.0156
		104	1.000	
		106	0.4345±0.0053	0.7730±0.0093

NOTE: $t_{\frac{1}{2}}$ for Ru^{103} = 39.7 days (Wright *et al.* 1957).
$t_{\frac{1}{2}}$ for Ru^{106} = 1.01 years average of 1.0 year (Schuman *et al.* 1956) and 1.02 years (Merritt *et al.* 1957).

Samples 1 and 5 were used for the determination of the relative yields of the zirconium isotopes shown in Table III. The natural contamination of Zr^{91}, Zr^{92}, Zr^{94}, and Zr^{96} yields was obtained from the abundance of Zr^{90}. It should be noted that the decay times used for the correction of the measured yields of Zr^{91} and Zr^{95} were not the same. The decay time for Zr^{95} represents the time until the mass spectrometric analysis. However, in the case of the Zr^{91} which grows in through its 58.0-day Y^{91} precursor, the decay time only includes the time until the dialysis of the sample. The relative yield of Zr^{91} was not determined using sample 1 since a large decay correction requires accurate values for the half-life of Y^{91} and also the time of separation. Sample 5 had decayed for over a year; hence the time of dialysis and half-life of the Y^{91} precursor were not critical.

The analysis of the fission molybdenum, shown in Table V, was complicated by the small amounts of natural molybdenum which were present in the tungsten filaments. The measured relative abundances of the fission molybdenum isotopes were corrected for this natural molybdenum contamination from the amount of mass 96 indicated by the mass spectrum. It was also

necessary to correct the measured abundance of Mo^{95} for the amounts of Zr^{95} and Nb^{95} which had not decayed to Mo^{95} at the time of analysis. For sample 9, this correction was too large for an accurate estimation of the mass 95 yield.

One half of sample 4 together with sample 6 was used in the analysis of fission ruthenium shown in Table VI. The absence of mass 99 proved that no natural ruthenium was present as a contaminant. The Ru^{103} abundance was too small to be measured with any degree of accuracy. The yield of Ru^{103} was determined relative to Ru^{106} using the isotope-diluted sample 9. Since the estimation of the relative yields from these measured abundances required the knowledge of two half-lives, that of Ru^{103} not being well known, the final relative yield is probably not as accurate as the mass spectrometric precision would indicate.

In addition to the relative yields shown in Tables II to VI, the relative yields of the rubidium isotopes were determined. The measured ratio Rb^{85}/Rb^{87} was 0.4517 ± 0.0036. A fission yield ratio of 0.6354 ± 0.0050 was obtained after correcting the Rb^{85} for the decay of the 10.27-year isomer of Kr^{85} during irradiation and the 0.3535 year from the end of irradiation to the time of analysis. It was assumed that 23% of the total mass chain decayed through the 10.27-year isomer while 77% decayed through the 4.36-hour isomer (Bergström 1951).

Table VII contains a summary of the relative yields of the isotopes of the various elements which were used in the determination of absolute fission yields. The values which were taken from Tables II to V are averages weighted according to the inverse square of the standard deviations.

TABLE VII

Relative yields of isotopes or various light fragments in the thermal neutron fission of Pu^{239}

Isotope	Relative yield	Isotope	Relative yield
Rb^{85}	0.6354 ± 0.0050	Ru^{101}	1.000
Rb^{87}	1.000	Ru^{102}	1.013 ± 0.014
		Ru^{103}	0.960
Sr^{88}	0.6530 ± 0.0071	Ru^{104}	1.003 ± 0.014
Sr^{89}	0.7846 ± 0.0089	Ru^{106}	0.773 ± 0.027
Sr^{90}	1.000		
		Mo^{95}	0.711 ± 0.022
Y^{89}	1.000	Mo^{97}	0.796 ± 0.015
Y^{91}	1.44 ± 0.02	Mo^{98}	0.829 ± 0.016
		Mo^{100}	1.000
Zr^{91}	0.656 ± 0.009		
Zr^{92}	0.790 ± 0.020		
Zr^{93}	1.000		
Zr^{94}	1.129 ± 0.017		
Zr^{95}	1.266 ± 0.022		
Zr^{96}	1.312 ± 0.018		

Samples 3, 8, and 9 were utilized in the determination of the absolute yields. The isotope dilution data along with the evaluated number of atoms of Cs^{133}, Rb^{87}, Sr^{90}, Mo^{98}, and Ru^{101} per gram of plutonium in each sample are shown in Tables VIII to XII. From the relative yields shown in Table VII

TABLE VIII

Mass spectrometric and isotope dilution data for Rb^{87} produced in the thermal neutron fission of Pu^{239}

Sample	Isotope	Ratio before isotope dilution	No. of atoms of isotope added per g of Pu^{239}, $\times 10^{15}$	Ratio after isotope dilution	Calculated fission yield, atoms $\times 10^{15}$/g Pu^{239}
9	85	1.000	4.736	1.000	—
	87	2.202±0.017	1.828	0.6874±0.0032	2.068
8	85	1.000	4.198	1.000	—
	87	2.199±0.017	1.620	0.7706±0.0052	2.472

TABLE IX

Mass spectrometric and isotope dilution data for Cs^{133} produced in the thermal neutron fission of Pu^{239}

Sample	Isotope	Ratio before isotope dilution	No. of atoms of isotope added per g of Pu^{239}, $\times 10^{19}$	Ratio after isotope dilution	Calculated fission yield, atoms $\times 10^{15}$/g Pu^{239}
9	133	1.000	5.938	1.000	16.01
	137	0.9329±0.0089	—	0.1421±0.0008	—
8	133	1.000	7.853	1.000	18.35
	137	0.9322±0.0089	—	0.1765±0.0010	—
3	133	1.000	5.938	1.000	1.145
	137	0.9233±0.0135	—	0.02144±0.00028	—

TABLE X

Mass spectrometric and isotope dilution data for Sr^{90} produced in the thermal neutron fission of Pu^{239}

Sample	Isotope	Ratio before isotope dilution	No. of atoms of isotope added per g of Pu^{239}, $\times 10^{19}$	Ratio after isotope dilution	Calculated fission yield, atoms $\times 10^{15}$/g Pu^{239}
9	88	0.6595±0.0062	1.274	3.307±0.022	—
	90	1.000	—	1.000	4.846
8	88	0.6599±0.0062	1.122	2.593±0.011	—
	90	1.000	—	1.000	5.849
3	88	1.191±0.012	0.6678	1.975±0.035	—
	90	1.000	—	1.000	0.3656

TABLE XI

Mass spectrometric and isotope dilution data for Mo^{98} produced in the thermal neutron fission of Pu^{239}

Sample	Isotope	Ratio before isotope dilution	No. of atoms of isotope added per g of Pu^{239}, $\times 10^{19*}$	Ratio after isotope dilution	Calculated fission yield, atoms $\times 10^{18}$/g Pu^{239}
9	96	—	3.461	1.000	—
	97	0.793±0.019	0.0483	0.3957±0.0034	—
	98	0.830±0.017	0.071	0.4429±0.0066	13.50
8	96	—	3.878	1.000	—
	97	0.793±0.019	0.0541	0.5045±0.010	—
	98	0.830±0.017	0.079	0.4149±0.0083	15.60

*Analysis of molybdenum solution used as isotope diluent: Mo^{96} 0.932±0.002; Mo^{97} 0.013±0.005; Mo^{94} 0.019±0.01.

TABLE XII

Mass spectrometric and isotope dilution data for Ru^{101} produced in the thermal neutron fission of Pu^{239}

Sample	Isotope	Ratio before isotope dilution	No. of atoms of isotope added per g of Pu^{239} $\times 10^{18}$	Ratio after isotope dilution	Calculated fission yield, atoms $\times 10^{18}$/g Pu^{239}
9	99	—	6.976	0.3042±0.0046	—
	101	1.000	9.338	1.000	13.60

and the number of atoms per gram of plutonium for one isotope of each fission element given in Tables VIII to XII, the number of atoms per gram of plutonium has been tabulated in columns 2, 4, and 6 of Table XIII for each of the samples.

The relative yields of the zirconium isotopes were normalized through the yield of the mass 95 chain whose value was obtained from the isotope dilution of fission molybdenum. In a similar manner, the relative yields of the krypton isotopes given by Fritze *et al.* (1958) were normalized to the rubidium isotopes through the yield of the mass 85 chain which was determined by isotope dilution.

For each of the isotope-diluted samples, the number of atoms of Cs^{133} per gram of plutonium was determined. Since the absolute yield of Cs^{133} has been evaluated as 6.90% (Fickel and Tomlinson 1959), it was possible to normalize the atom yields of the isotopes of the other elements to percentage yields.

The final values shown in column 8, Table XIII, and graphically represented in Fig. 1 consist of the averages of the percentage yields in columns 3, 5, and 7. Radiochemical yields for masses 109, 111, and 112 (Katcoff 1958) and the yields from the interpolation and extrapolation of a mass–yield plot are also included in Table XIII.

TABLE XIII

Cumulative fission yields of the light fragments in the thermal neutron fission of Pu^{239} normalized to the 6.90% Cs^{133} yield

Isotopic mass	Sample 3		Sample 8		Sample 9		Average % yield
	Atoms×10^{18}	% yield	Atoms×10^{18}	% yield	Atoms×10^{18}	% yield	
72–82							0.59*
Kr^{83}							0.29
Kr^{84}							0.47
Rb^{85} (Kr^{85})			1.460	0.5456	1.262	0.5251	0.535
Kr^{86}							0.75
Rb^{87}			2.487	0.9291	0.2150	0.8942	0.912
Sr^{88}	0.2387	1.438	3.819	1.440	3.164	1.368	1.43
Sr^{89}	0.2868	1.728	4.589	1.726	3.802	1.639	1.71
Sr^{90}	0.3656	2.203	5.849	2.199	4.846	2.089	2.16
Zr^{91}							2.59
Zr^{92}							3.12
Zr^{93}							3.94
Zr^{94}							4.45
Mo^{95} (Zr^{95})			13.37	5.025	11.58	4.991	4.99
Zr^{96}							5.13
Mo^{97}			14.97	5.630	12.97	5.590	5.61
Mo^{98}			15.60	5.861	13.50	5.818	5.84
99							6.44*
Mo^{100}			1.882	7.072	1.629	7.020	7.05
Ru^{101}					13.60	5.860	5.86
Ru^{102}					13.78	5.939	5.94
Ru^{103}					13.06	5.626	5.63
Ru^{104}					13.64	5.877	5.88
105							5.50*
Ru^{106}					1.051	4.530	4.53
107							3.40*
108							2.44*
109							1.50†
110							0.76*
111							0.27†
112							0.10†
113							0.080*
114							0.060*
115							0.041*
116–118							0.122*
Cs^{132}	1.45	6.90	18.35	6.90	16.01	6.90	
Total % yield							100.12

*Interpolated values.
†Radiochemical yields.

DISCUSSION

The relative yields obtained for the light mass fragments are less precise than those of the previously published relative yields of the heavy mass fragments (Fickel and Tomlinson 1959). Such factors as the presence of molybdenum in the tungsten filament and large half-life corrections have reduced the precision of the relative yields. In spite of such factors, however, precisions between 1 and 2% have been obtained in most cases.

The accuracy of the absolute yield values also depends on the normalization of the relative yields. In the cases of the rubidium, strontium, molybdenum, and ruthenium, this was achieved by isotope dilution. The reproducibility of the analyses as shown by Table XIII is within 4% for most cases. The zirconium

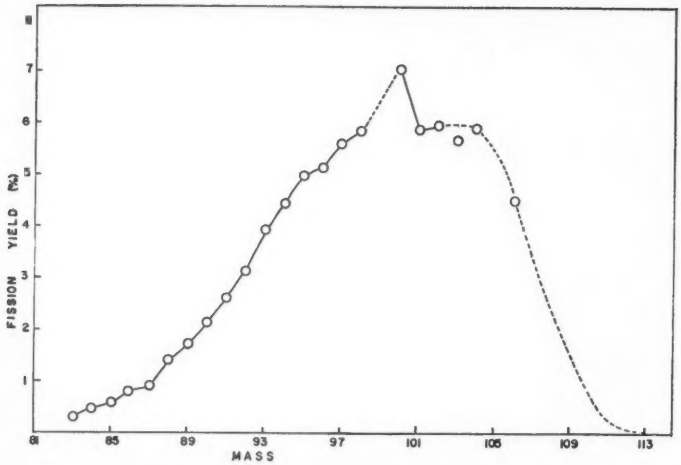

FIG. 1. Light mass yields in thermal neutron fission of Pu^{239}.

was not isotope-diluted, but the relative yields were normalized to those of the other elements through the yield of the mass 95 chain obtained from molybdenum. This procedure was used rather than direct isotope dilution because absorption characteristics of this element in solution make the equilibration of the zirconium fission product and isotope diluent zirconium difficult. It will be noted from Table XIII that the yield of Zr^{91} is 1.52 times greater than the yield of Sr^{89}. The relative yields of the mass 91 and 89 chains may also be obtained from the relative yields of the yttrium isotopes as shown in Table IV. The value obtained in this manner is 1.44 ± 0.02, but the precision only includes the uncertainty introduced from the mass spectrometric observations and not the systematic errors introduced by the large half-life corrections. If the factor 1.44 had been used to normalize the Zr^{91} yield to that of Sr^{89}, the zirconium yields would have been about 5.5% lower than those given in Table XIII. This inconsistency would be substantially removed if the yttrium ratios had been corrected for decay using 57 instead of 58 for the half-life of Y^{91}.

To compare the Rb^{85} yield obtained in this work with the Kr^{85} yield found by Fritze *et al.* (1958) it is necessary to assume the branching ratio for the 4.4-hour Kr^{85m}. If it is assumed that 77% of the short-lived krypton isomer decays directly to rubidium, it is found that the 0.55% yield given by Fritze *et al.* becomes 0.539, which is in exact agreement with that found in the present work. This has provided a confirmation of the branching ratio reported by Bergström (1951), but is slightly greater than the value estimated by Blades and Thode (1955), who found that 78% of the Kr^{85m} decayed directly to Rb^{85}.

Krizhanskii and Murin (1958) have published yields of Sr^{88} and Sr^{90} formed in the thermal neutron fission of Pu^{239}. Both relative and absolute yields of these two isotopes were significantly different from those found in this work. These authors have given insufficient experimental detail to assess the reason for the differences.

The summation of the yields of the light mass fragments given in Table XIII totals 100.13%, which assures confidence in the values. The accuracy of the absolute cumulative fission yields shown in Table XIII is considered to be better than 4%.

ACKNOWLEDGMENTS

We wish to thank Atomic Energy of Canada Limited for the neutron irradiations and the National Research Council of Canada for financial assistance.

REFERENCES

BERGSTRÖM, I. M. 1951. Siegbahn Communication, Volume XX, Uppsala 307.
BLADES, A T. and THODE, H. G. 1955. Z. Naturforsch. **10***a*, 838.
CORK, J. M., LEBLANC, J. M., MARTIN, D. W., NESTER, W. H., and BRICE, M. K. 1953. Phys. Rev. **90**, 579.
ENGELKEMEIR, D. W., Brady, E. L., and STEINBERG, E. P. 1951. NNES-PPR **9**, 722.
FICKEL, H. R. and TOMLINSON, R. H. 1959. Can. J. Phys. **37**, 531.
FRITZE, K., MCMULLEN, C. C., and THODE, H. G. 1958. Second International Conference on the Peaceful Uses of Atomic Energy, Paper 187.
KAHN, B. and LYON, W. S. 1955. Phys. Rev. **98**, 58.
KATCOFF, S. 1958. Nucleonics, **16** (4), 78.
KRIZHANSKII, L. M. and MURIN, A. N. 1958. The Soviet Journal of Atomic Energy (English Trans.) **4**, 95.
MERRITT, W. F., CAMPION, P. J., and HAWKINGS, R. C. 1957. Can. J. Phys. **35**, 16.
PETRUSKA, J. A., MELAIKA, E. A., and TOMLINSON, R. H. 1955. Can. J. Chem. **33**, 640.
SCHUBERT, J. and CONN, E. E. 1949. Nucleonics, **4** (6), 2.
SCHUMAN, R. P., JONES, M. E., and MEWHERTER, A. C. 1956. J. Inorg. & Nuclear Chem. **3**, 160.
WILES, D. M. and TOMLINSON, R. H. 1955. Can. J. Phys. **33**, 133.
WILES, D. M., PETRUSKA, J. A., and TOMLINSON, R. H. 1956. Can. J. Chem. **33**, 227.
WRIGHT, H. W., WYATT, E. I., REYNOLDS, S. A., LYON, W. S., and HANDLEY, T. H. 1957. Nuclear Sci. and Eng. **2**, 157.

THE CUMULATIVE FISSION YIELDS OF 21 HEAVY MASS NUCLIDES PRODUCED IN THE THERMAL FISSION OF Pu^{239} [1]

H. R. FICKEL[2] AND R. H. TOMLINSON

ABSTRACT

Mass spectrometric analysis of cesium, barium, cerium, neodymium, and samarium produced in the thermal fission of Pu^{239} has made possible the determination of the cumulative yields of 17 mass chains. With previously published mass spectrometric yields of four xenon isotopes normalized to the present data a total of 21 cumulative yields are reported.

INTRODUCTION

Radiochemically determined yields of nuclides formed in the thermal neutron fission of Pu^{239} have been summarized by Steinberg and Freedman (1951) and Steinberg and Glendenin (1955). The summation of those for the heavy mass fragments assuming a smooth curve totals only 93% indicating considerable error in either the measured values or those interpolated from the smooth mass–yield curve. Mass spectrometric values for the absolute yields of the heavy fragments were published by Wiles and Tomlinson (1956) and later by Krizhanskii *et al.* (1957). In the work of Wiles and Tomlinson (1956) only 80% of the fission product activity was recovered in the procedure of dissolving the irradiated PuO_2. It was pointed out in the discussion of this work that the yields reported would be inaccurate if the losses of the various elements were not equal. The yields obtained by Krizhanskii *et al.* (1957), although in essential agreement with those of Wiles, can not be considered completely independent and hence a confirmation of Wiles' data, since only relative yields were actually measured and these yields normalized to Wiles' absolute yield values at Nd^{143} and Cs^{137}.

The present work is a careful redetermination of the yields reported by Wiles *et al.* together with a further yield of Ba^{138}.

EXPERIMENTAL

Two different samples were used to determine the thermal neutron fission yields for plutonium. The first sample was 10.12 mg PuO_2 (96.1% Pu^{239}) sealed in a quartz capsule. This was irradiated along with a flux monitor consisting of 1.15-mg Co wire, 0.13 mm in diameter, for 51.34 days at a flux of 3.36×10^{12} thermal neutrons per square centimeter per second in the NRX reactor, Chalk River. Eight months after the sample had been removed from the reactor it was completely dissolved in a platinum crucible by a continuous hot HF–HCl treatment for approximately 7 days. The quartz capsule was then washed several times with HF until all the activity had been removed. Without any chemical separation, a small fraction (less than 1%) of the solution was analyzed with a mass spectrometer for the presence of stable isotope con-

[1]Manuscript received May 11, 1959.
Contribution from Chemistry Department, McMaster University, Hamilton, Ontario.
[2]Holder of Canadian Industries Limited Fellowship, 1957–1958. Holder of an International Nickel Company Limited Fellowship, 1958–1959.

tamination of each of the fission product elements cesium, cerium, neodymium, and samarium. The remainder of this solution was isotope-diluted using the method previously described by Petruska *et al.* (1955). The mass spectrometer was a 10-in. radius, 90° sector, solid source instrument equipped with magnetic scanning and a 10-stage electron multiplier assembly.

A second sample weighing 41 mg was half of a Pu–Al alloy disk which had been irradiated for 23.88 days at a flux of 2.51×10^{12} thermal neutrons per square centimeter per second in the NRX reactor, Chalk River. The alloy contained 13.9% Pu of which 96.1% was Pu^{239}. In order to calculate the number of fissions in this sample it was necessary to determine the neutron flux and the effective cross section. This was accomplished in the following manner.

The Pu–Al alloy was enclosed in an aluminum capsule about 2.5 cm in length. Cobalt wire flux monitors, 0.13 mm in diameter and 1.56 mg and 1.66 mg in weight, were placed at each end of the capsule. The neutron flux was determined from the activity induced in the cobalt which was measured in a well-type ionization chamber relative to cobalt standards whose absolute disintegration rate had been previously determined by absolute beta counting.

The effective cross section of the Pu^{239} requires a knowledge of the neutron temperature. A neutron temperature monitor, consisting of 25 μg of samarium evenly deposited on aluminum foil, was wrapped around the inside of the capsule.

The mass spectrometric ratio of Sm^{150}/Sm^{149} after the irradiation was used to obtain the neutron temperature as discussed below.

Sixteen months after irradiation this sample was dissolved in distilled HNO_3. The fission products were analyzed with the mass spectrometer both before and after isotope dilution in the same manner as for the PuO_2 sample. In addition, analysis of fission Ba^{138} was carried out for this sample using a solution of enriched Ba^{134}. The concentrations of the barium isotopes in the enriched Ba^{134} solution were determined by means of isotope dilution with a known quantity of natural barium.

EXPERIMENTAL RESULTS

The observed mass spectrometric ratios of the fission products together with the relative fission yields of the isotopes of cesium, neodymium, cerium, and samarium are shown in Tables I to IV, respectively, as well as previously reported values. Tables VI to IX contain the isotope dilution data along with

TABLE I

Relative yields of the cesium isotopes produced in the thermal neutron fission Pu^{239}

Isotope	Mass spectrometric ratio	Relative fission yield		
		This work	Literature	
			Wiles (1956)	Krizhanskii (1957)
Cs^{133}	1.000	1.000	1.00	1.000
Cs^{135}*	0.7813±0.0094	1.05±0.15	1.05±0.15	2.377±0.24
Cs^{137}†	0.915±0.012	0.940±0.013	0.994±0.005	2.242±0.020

*Corrected for 3.45×10^6-barn neutron absorption cross section of Xe^{135} (Petruska *et al.* 1955).
†Corrected for 26.6-year half-life of Cs^{137} (Wiles *et al.* 1955).

TABLE II

Relative yields of the neodymium isotopes in the thermal neutron fission of Pu^{239}

Isotope	Mass spectrometric ratio	Relative fission yield		
		This work	Literature	
			Wiles (1956)	Krizhanskii (1957)
Nd^{143}*	1.000	1.000	1.00	1.00
Nd^{144}†	0.424±0.005	0.841±0.010	0.836±0.006	0.840±0.006
Nd^{145}	0.685±0.008	0.685±0.008	0.681±0.005	0.666±0.002
Nd^{146}	0.563±0.008	0.563±0.008	0.561±0.005	0.557±0.002
Nd^{148}	0.375±0.006	0.375±0.006	0.379±0.002	0.362±0.005
Nd^{150}	0.223±0.003	0.223±0.003	0.219±0.002	0.220±0.002

*Correction for 334-barn neutron absorption cross section of Nd^{143} was insignificant in this work (Walker and Thode 1953).

†Corrected for 278-day half-life of Ce^{144}.

TABLE III

Relative yields of cerium isotopes produced in the thermal neutron fission of Pu^{239}

Isotope	Mass spectrometric ratios	Relative fission yield		
		This work	Literature	
			Wiles (1956)	Krizhanskii (1957)
Ce^{140}	1.12±0.01	1.12±0.01	1.11±0.02	0.85±0.01
Ce^{142}	1.00	1.00	1.00	1.00
Ce^{144}*	0.380±0.003	0.773±0.006	0.77±0.02	0.79±0.04

*Corrected for 278-day half-life of Ce^{144}.

TABLE IV

Relative yields of samarium isotopes produced in the thermal neutron fission of Pu^{239}

Isotope	Mass spectrometric ratios	Relative fission yield		
		This work	Literature	
			Wiles (1956)	Krizhanskii (1957)
Sm^{147}*	0.4594±0.0068	1.846±0.027	1.88±0.02	1.838±0.048
Sm^{149}	1.00	1.209±0.003	1.209	1.209
Sm^{150}	0.2089±0.0029			
Sm^{151}†	0.7410±0.0067	0.7410±0.0074	0.736±0.014	0.764±0.01
Sm^{152}†	0.5685±0.0045	0.5685±0.0045	0.595±0.014	0.500±0.01
Sm^{154}	0.2719±0.0035	0.2719±0.0035	0.265±0.006	0.193±0.004

*Corrected for 2.52-year half-life of Pm^{147} (Melaika *et al.* 1955).

†Corrected for 12,800-barn cross section of Sm^{151} (Melaika *et al.* 1955).

TABLE V

Mass spectrometric isotope dilution data for Ba^{138} produced in the thermal neutron fission of Pu^{239}

	Isotope		
	134	136	138
Atoms added per gram of plutonium $\times 10^{17}$	6.486	0.9485	1.940
Relative abundances in natural barium	0.242	0.781	7.166
Mass spectrometric ratio after isotope dilution	0.2484±0.0025	0.1097±0.0019	1.000
Atoms of fission Ba^{138} per gram of plutonium $\times 10^{17}$ in sample 2			6.575

TABLE VI

Mass spectrometric and isotope dilution data for Ce^{142} produced in the thermal neutron fission of Pu^{239}

	Isotope		
	140	142	144
Mass spectrometric ratios			
1		1.000	0.3694±0.0031
2	1.000	0.6668±0.0051	
Ratio after dilution with natural cerium			
1. 2.576×10^{19} atoms per gram of plutonium		1.000	0.09501±0.00080
2. 1.685×10^{18} atoms per gram of plutonium	1.000	0.3204±0.0030	
Atoms of fission Ce^{142} per gram of plutonium $\times10^{17}$			
1		9.880	
2		5.299	

TABLE VII

Mass spectrometric and isotope dilution data for Sm^{151} produced in the thermal neutron fission of Pu^{239}

	Isotope	
	151	152
Mass spectrometric ratios		
1	1.000	0.870±0.018
2	1.000	0.864±0.010
Ratio after dilution with natural samarium		
1. 7.660×10^{18} atoms Sm per gram of plutonium	1.000	13.95±0.40
2. 2.930×10^{18} atoms Sm per gram of plutonium	1.000	9.72±0.19
Atoms of fission Sm^{151} per gram of plutonium $\times10^{17}$*		
1	1.638	
2	0.9288	

*Corrected for 12,800-barn cross section of Sm^{151} (Melaika *et al.* 1955).

TABLE VIII

Mass spectrometric and isotope dilution data for Cs^{133} produced in the thermal neutron fission of Pu^{239}

	Isotope	
	133	137
Mass spectrometric ratios		
1	1.000	0.923±0.013
2	1.000	0.907±0.013
Ratio after dilution with natural Cs		
1. 5.932×10^{19} atoms per gram of plutonium	1.000	0.0214±0.0003
2. 9.970×10^{18} atoms per gram of plutonium	1.000	0.0610±0.0004
Atoms of fission Cs^{133} per gram of plutonium $\times10^{18}$		
1	1.405	
2	0.7193	

TABLE IX

The mass spectrometric and isotope dilution data for Nd^{143} produced in the thermal neutron fission of Pu^{239}

	Isotope	
	142	143
Mass spectrometric ratios		
1		1.000
2		1.000
Ratio after dilution with natural neodymium		
1. 8.735×10^{18} atoms per gram of plutonium	2.026 ± 0.015	1.000
2. 2.578×10^{18} atoms per gram of plutonium	0.8744 ± 0.0078	1.000
Atoms of fission Nd^{143} per gram of plutonium $\times10^{18}$		
1		1.076
2		0.4856

the evaluated number of atoms of Ce^{142}, Sm^{149}, Cs^{133}, and Nd^{143} per gram of plutonium in each sample. From the relative yields for each of the elements given in Tables I to IV and the absolute number of atoms of one isotope of each of these elements given in Tables VI to IX, the number of atoms of each fission nuclide per gram of plutonium has been tabulated in columns 2 and 4 of Table X for each of the two samples.

TABLE X

Cumulative yields based on calculated number of fissions

	PuO_2		Pu–Al alloy	
Atomic number	No. of atoms/g Pu, $\times10^{18}$	% yield	No. of atoms/g Pu, $\times10^{17}$	% yield
118–130		5.70*		5.70*
131	.7666	3.83	3.925	3.70
132	1.070	5.34	5.477	5.16
133	1.405	7.02	7.193	6.77
134	1.519	7.59	7.775	7.32
135	1.477	7.38	7.552	7.11
136	1.349	6.74	6.907	6.51
137	1.320	6.60	6.763	6.37
138		6.43*	6.574	6.19
139		6.05		5.92*
140	1.110	5.55	5.953	5.61
141		5.14		5.31*
142	0.9880	4.94	5.299	4.99
143	0.9081	4.53	4.856	4.57
Ce^{144}				
Nd^{144}	0.7637	3.81	4.09	3.86
145	0.6220	3.11	3.326	3.13
146	0.5113	2.56	2.734	2.58
147	0.4064	2.03	2.056	1.94
148	0.3405	1.70	1.822	1.72
149	0.2661	1.33	1.346	1.27
150	0.2023	1.01	1.083	1.02
151	0.1638	0.82	0.9288	0.78
152	0.1258	0.63	0.6364	0.60
153		0.45*		0.45*
154	0.05988	0.299	0.3029	0.285
155		0.18*		0.17*
156		0.08*		0.08*
		100.85		99.11

*Assumed yields.

The yields of the xenon isotopes given by Fleming and Thode (1956) are normalized to the cesium isotopes by means of the factor 0.925 ± 0.010 given by these authors for the ratio Xe^{133}/Xe^{134}. In the mass region below mass 130, radiochemical yields have been used where possible. Other yields appearing in Table X including masses 139 and 141, which have not been obtained directly, have been interpolated from a plot of yield versus mass.

The yield of the 144 mass chain may be obtained from both the cerium and neodymium isotope dilutions. For sample 1, the value obtained from the neodymium is 15% higher than from the cerium. It may be seen from Table IX that for this sample too much natural neodymium was used in the isotope dilution so that the ratio of Nd^{142}/Nd^{143} after isotope dilution was very nearly that of natural neodymium. For such conditions the accuracy of the determination of the number of fission Nd^{143} is greatly reduced. In Table IX, therefore, the values for the neodymium isotopes in sample 1 have been obtained from the relative yields shown in Table II and the number of atoms of mass 144 taken from Ce^{144} shown in Table VI. For the plutonium–aluminum alloy sample identical yields at mass 144 were obtained from both the cerium and neodymium isotope dilutions. This agreement is obtained when a value of 278-day half-life for Ce^{144} is assumed for the growth and decay corrections of the observed mass spectrometric data of both the neodymium and cerium given in Tables II and III respectively.

The yield of Ba^{138} was determined only for the Pu–Al alloy sample using the isotope dilution data shown in Table V. The number of fission atoms of Ba^{138} per gram of plutonium is given in Tables V and X.

Two methods may be used to obtain absolute cumulative fission yields from the data given in columns 2 and 4 of Table X. In one method the absolute number of fissions is calculated from the irradiation data and the fission cross section of Pu^{239}, and in the other method the relative yields are adjusted so that they total 100%. The absolute number of fissions in the Pu^{239} may be calculated using the following relation (1):

$$N_f = N_{239} \times (nv)t \times \hat{\sigma}_f \times S \tag{1}$$

where N = number of atoms of the nuclide,
N_f = number of fissions,
N_{239} = number of atoms of Pu^{239} in the sample,
$\hat{\sigma}_f$ = effective neutron fission cross section of Pu^{239} in cm^2,
$(nv)t$ = integrated flux in neutrons cm^{-2},
S = the flux self-shielding correction for the irradiated samples.

In equation (1), the integrated flux $(nv)t$ and the effective neutron fission cross section of Pu^{239} require determination. The former can be related to the disintegration rate, dN_{60}/dt, of the cobalt monitors according to equation (2):

$$(nv)t = \frac{dN_{60}}{dt} \times \frac{1}{\lambda N_{59} \hat{\sigma}_{Co} S} \tag{2}$$

where λ = decay constant for $Co^{59} = 4.18 \times 10^{-9}$ sec^{-1},
N_{59} = number of cobalt atoms,
$\hat{\sigma}_{Co}$ = effective cross section for cobalt in cm^2,
S = the flux self-shielding correction for cobalt wire.

The effective neutron cross section, $\hat{\sigma}$, of any nuclide is a function of the neutron energy distribution and the variation of its cross section with energy. The value of $\hat{\sigma}$ may be calculated from the following expression given by Westcott (1958):

$$\hat{\sigma} = \sigma_0 (g + rs) \tag{3}$$

where σ_0 = the monokinetic cross section at 2200 m sec^{-1},

g represents the departure of the nuclide's cross section from $1/V$ law in terms of its effect for a Maxwellian neutron spectrum,

r = epithermal index as defined by Westcott (1958),

s characterizes the departure of the nuclide's cross section from a $1/V$ law in the epithermal region.

For the cobalt monitors the r value was taken as 0.01, $\sigma_0 = 36.5$ barns (Jervis 1958), and 123° C for the apparent temperature of the Maxwellian component of the neutron distribution (see calculation below). Using the values of g and s taken from tables given by Westcott (1958) one obtains a value of 36.9 barns for the effective neutron cross section of Co^{59}.

Using the methods previously described (by Petruska *et al.* (1955)) 0.977 self-shielding corrections were made for the cobalt monitors. With these the measured specific activities of the cobalt monitors shown in Table XII and the values of the neutron flux shown in Table XII have been calculated with equation (2).

The value of the effective fission cross section, $\hat{\sigma}_f$, for Pu^{239} is dependent on the apparent neutron temperature. The apparent neutron temperature may be calculated from the effective cross section of Sm^{149}. This was obtained from the measured ratio of the samarium isotopes in the irradiated samarium monitor using equation (4).

$$\left[\frac{Sm^{150}}{Sm^{149}} = 1.54(\exp \hat{\sigma}_{Sm^{149}}(nv)t) - 1\right] \tag{4}$$

where 1.86 = the natural ratio of Sm^{149}/Sm^{150} in the unirradiated sample,

Sm^{150}/Sm^{149} = the observed ratio after irradiation.

For the plutonium–aluminum alloy sample, the observed value of Sm^{150}/Sm^{149} was found to be 1.35 ± 0.01 and hence $\hat{\sigma}_{Sm^{149}} = 81{,}500$ barns. A value of 123° C for the neutron temperature may then be estimated from equation (3) using 42,200 barns for σ_0 (Bidinosti *et al.* 1958), $r = 0.01$, and values of g and s given as a function of temperature by Westcott (1958). For this temperature a value of 872 barns is estimated for the effective fission cross section of Pu^{239} from equation (3) using 750 barns for the 2200 m/sec fission cross section and the values of g and s tabulated by Westcott (1958).

Although the PuO_2 sample did not have a samarium monitor, it was irradiated in the same position in the NRX reactor and the fission cross section for plutonium has been assumed to have the same value. With this value for the effective cross section of Pu^{239}, the self-shielding corrections calculated in the same manner as for the cobalt monitors and the integrated fluxes given in Table XII, the number of fissions per gram of plutonium shown in this table have been calculated using equation (1).

With the yields in atoms per gram of plutonium given in columns 2 and 4 of Table X and the number of fissions per gram of plutonium given in Table XII, the yields shown in columns 3 and 5 in Table X have been obtained.

The method of adjusting the absolute cumulative yields of the heavy mass curve to add to 100% is accomplished by taking the ratios of 100 times the number of atoms per gram of plutonium which are given in columns 2 and 4 of Table X to the total numbers of fissions per gram of plutonium which are the summations of columns 2 and 4 of Table X.

The final fission yields shown in Table XI and represented graphically in Fig. 1 have been obtained in this manner.

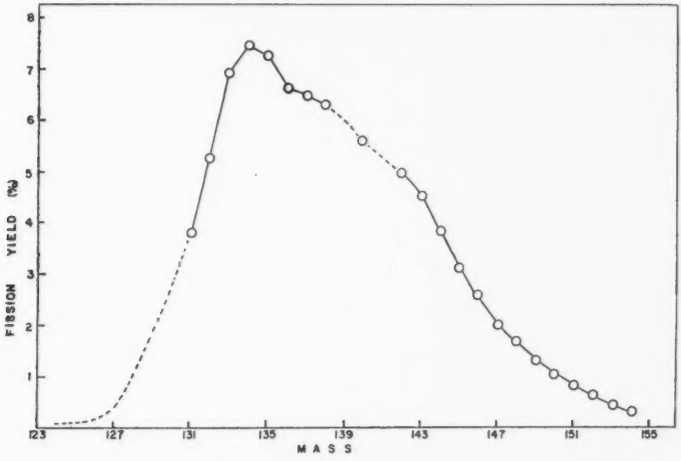

FIG. 1. Heavy mass yields in thermal neutron fission of Pu^{239}.

DISCUSSION

The accuracy of the relative yields of the isotopes of a given element depends only on the accuracy of the directly determined mass spectrometric measurements whereas the fission yields also depend on isotope dilution measurements. The precision of the relative yields given in Tables I to IV are in each case better than 1% and agree within these limits with the values previously published (Wiles and Tomlinson 1956; Krizhanskii *et al.* 1957) except at three mass regions. The most serious difference is the ratio of Cs^{133}/Cs^{137} shown in Table I. Since Cs^{133} is the stable isotope which occurs in nature it may be considered that high values of this ratio are the result of stable contamination. In the previous determination from this laboratory (column 4, Table I), only partial recovery of the fission products was achieved. Recent unpublished work in this laboratory has established that the mobility of the 5-day Xe^{133} precursor to Cs^{133} can materially alter fission yield ratios of cesium isotopes in oxide samples.

TABLE XI

Cumulative yields and other literature values

Atomic number	% yield				
	PuO_2	Pu–Al alloy	Average	Wiles (1956)	Steinberg *et al.* (1955)
118–130	5.65*	5.75*	5.70*	5.38	
131	3.80	3.73	3.77	2.71	3.6
132	5.30	5.21	5.26	3.79	4.9
133	6.96	6.83	6.90	4.97	5.0
134	7.52	7.39	7.46	5.37	
135	7.32	7.17	7.25	5.22	5.5
136	6.69	6.56	6.62	4.77	
137	6.54	6.42	6.48	4.94	5.8
138	6.37*	6.25	6.31	5.38	
139	6.00*	5.97*	5.99*	6.61	5.4
140	5.50	5.66	5.58	7.36	5.36
141	5.10*	5.36*	5.23*	6.94	4.9
142	4.90	5.03	4.97	6.62	
143	4.50	4.61	4.56	5.98	5.1
144	3.78	3.89	3.84	5.00	3.7
145	3.08	3.16	3.12	4.07	
146	2.53	2.60	2.57	3.36	
147	2.02	1.96	1.99	2.81	
148	1.69	1.73	1.71	2.27	
149	1.32	1.28	1.30	1.81	
150	1.00	1.03	1.02	1.31	
151	0.814	0.790	0.802	1.10	
152	0.625	0.606	0.616	0.88	
153	0.45*	0.45*	0.45*	0.64	0.39
154	0.297	0.289	0.293	0.40	
155	0.17*	0.17*	0.17*	0.30	
156	0.08*	0.08*	0.08*	0.08	0.12
Total	100%	100%	100%	100%	93%

*Assumed yields.

NOTE: Summation of measured yields together with values interpolated from smooth mass–yield curve by Steinberg *et al.* (1955) totals 93%.

TABLE XII

Number of fissions in the plutonium samples

Sample	Specific activity of cobalt monitors, mc/g	$(nv)t$, n/cm²	Self-shielding correction	Number of fissions/g of Pu^{239}
PuO_2	630.7	1.525×10^{19}	0.6043	2.001×10^{19}
Pu–Al Alloy	216*	5.19×10^{18}	0.930	1.062×10^{19}

*Average for two monitors.

The value obtained by Krizhanskii *et al.* (1957) can not be assessed without further information, but the new value presented in Table I has been confirmed with measurements from several entirely different irradiations. A similar type of variation, but to a lesser extent, has also been observed at mass 140 (see Table III) which apparently does not depend on stable contamination.

A further difference is observed in the samarium yields at masses 152 and 154 (see Table IV). The yields given by Krizhanskii *et al.* (1957) were corrected

assuming Sm^{148} is contamination arising from natural samarium. In fact the Sm^{148} was probably produced by decay of Pm^{148} formed by an (n, γ) reaction with Pm^{147} and hence this correction should not have been made. The values of Krizhanskii *et al.* (1957) without correction for Sm^{148} correspond closely to the values obtained in this work.

Fritze and co-workers (1958) in their simultaneous determinations of xenon and krypton from the same Pu–Al alloy sample obtain a cumulative fission yield of 3.79 ± 0.11 for Xe^{131}. This is in good agreement with the value of 3.77 obtained in this work from the measured yield of Cs^{133} and the relative yields of Xe^{133} and Xe^{131} previously given by Fleming and Thode (1956).

The final values of the cumulative fission yields of Pu^{239} given in Table XI have been normalized so that the yields total 100%. The values given in Table X depend on the calculation of the total number of fissions occurring in each sample. In the case of the PuO_2 sample, where the neutron temperature was not measured (hence the fission cross section doubtful) and where the self-shielding correction amounted to about 40%, it is considered fortuitous that the yields shown in Table X total 100.85%. For this sample the values shown in Table XI are therefore to be preferred. In the case of the Pu–Al alloy sample these factors were more carefully controlled and therefore the 99.11% summation of the yields in Table X could well be a measure of the cumulative errors in the several determinations or in the values of the few yields which have been assumed. The final values for this sample shown in Table XI have nevertheless been normalized to 100% since they are then independent of the calculated number of fissions, a factor which is dependent on the relative cross sections of Pu^{239} and Co^{59} and on the self-shielding correction. The agreement with the yields shown in Table X is taken as a measure of the absence of loss or fractionation of fission products from the sample.

The yields of Wiles *et al.* (1956), also shown in Table XI, are now assumed to be in error from fractionation which occurred in the partial extraction of the fission products from the PuO_2. The radiochemical yields summarized by Steinberg *et al.* (1955) are difficult to compare with the present values since their summation is only 93%.

The values of the yields obtained from the two independent determinations shown in columns 2 and 3 of Table XI agree to better than 2% at most masses and the average values shown in column 4 of Table XI are considered to have an absolute accuracy of better than 3% at each mass.

ACKNOWLEDGMENTS

We wish to thank Atomic Energy of Canada Limited for the neutron irradiations and the National Research Council of Canada for financial assistance.

REFERENCES

Bidinosti, D. R., Fickel, H. R., and Tomlinson, R. H. 1958. International Conference on Peaceful Uses of Atomic Energy, Geneva, paper P/201.

Case, K. M., De Hoffmann, F., and Placzek, G. 1953. Introduction of the theory of neutron diffusion. Vol. 1 (U. S. Government Printing Office, Washington, D. C.).

FLEMING, W. H. and THODE, H. G. 1956. Can. J. Chem. **34**, 193.
FRITZE, K., MCMULLEN, C. C., and THODE, H. G. 1958. Second International Conference on the Peaceful Uses of Atomic Energy, paper 187.
JERVIS, R. F. 1958. Atomic Energy of Canada Ltd., Chalk River, Ontario (private communication).
KRIZHANSKII, L. M., MALYI, YA, MURIN, A. N., and PREOBRAZHENSKII, B. K. 1957. Soviet J. Atomic Energy, **2**, 334.
MELAIKA, E. A., PARKER, M. T., PETRUSKA, J. A., and TOMLINSON, R. H. 1955. Can. J. Chem. **33**, 830.
PETRUSKA, J. A., MELAIKA, E. A., and TOMLINSON, R. H. 1955. Can. J. Phys. **33**, 640.
STEINBERG, E. P. and FREEDMAN, M. S. 1951. National Nuclear Energy, Ser. 9, paper 219.
STEINBERG, E. P. and GLENDENIN, L. E. 1955. A/Conf. 15/P/614.
WALKER, W. H. and THODE, H. G. 1953. Phys. Rev. **90**, 448.
WESTCOTT, C. H. 1958. Effective cross section values for well-moderated thermal reactor spectra, Atomic Energy of Canada Limited Report 670.
WILES, D. M., PETRUSKA, J. A., and TOMLINSON, R. H. 1956. Can. J. Chem. **34**, 227.
WILES, D. M. and TOMLINSON, R. H. 1955. Phys. Rev. **99**, 188.

THE SUPERCONDUCTING TRANSITION IN POLYCRYSTALLINE TIN[1]

R. A. Aziz and D. C. Baird

ABSTRACT

The influence of grain size on the breadth of the superconducting transition in polycrystalline tin has been studied. The transition has been detected using an a-c. induction method. A range of grain sizes from 0.2 mm to 10 mm was used and the corresponding range in transition breadth is from 75 to 18 millidegrees. The influence of the grain boundaries is to broaden all the transition curves towards higher temperatures from a well-defined end point which is common to all the curves.

INTRODUCTION

In view of the interest attached to the influence of lattice imperfections on the superconducting transition and the apparent lack of information on the role of grain boundaries specifically, experiments have been done to study the effect of grain size on the superconducting transition. Work on thin films has shown a marked dependence of the superconducting properties on the lattice structure but has not apparently isolated the influence of grain boundaries alone. The only work done hitherto on bulk specimens seems to be that of de Haas and Voogd (1931), who quote results for only three samples and, of these, only two are of related purity. No figures for the actual grain size are given. The problem of the influence of grain boundaries on the superconducting transition is of interest, not only for its own sake in considering the mechanism of the transition but also in aiding the evaluation of experiments on other properties of superconductors which are performed on polycrystalline materials. The aim of the present work, therefore, is to repeat and extend the measurements of de Haas and Voogd in an attempt to clarify the nature of the transition broadening found in polycrystals.

SPECIMENS

The specimens were made from zone-refined tin obtained from the Department of Physical Metallurgy, University of Toronto, and two samples taken from the same bar were used. One was cut from the original bar so as to be composed almost entirely of a single crystal with only one longitudinal grain boundary. The other was cut at random and severely worked by hammering so as to achieve the smallest possible grain size. Each was turned into a cylinder approximately 5 mm in diameter and 5 cm long. The worked surface produced by machining was etched away, thereby simultaneously revealing the grain structure for grain-size measurements. Each specimen was annealed at 100° C for 2 hours to ensure that the lattice within the grains was as free of stress as

[1]Manuscript received May 8, 1959.
Contribution from the Department of Physics, Royal Military College of Canada, Kingston, Ontario. This research was supported in part by the Defence Research Board of Canada, under Grant No. 9510-21, Project No. D48-95-10-21.

possible. After measurements of its superconducting transition as described below this second specimen was annealed at a temperature just below the melting temperature for the time required to increase the average grain diameter. The transition experiments and grain-growth procedure were repeated on the specimen until no further grain growth could be achieved.

METHOD

The transitions were detected magnetically by a method described by Webber, Reynolds, and McGuire (1949). The specimen was mounted vertically in a liquid helium bath and was enclosed in a close-fitting secondary coil. An oscillating longitudinal magnetic field was produced by a solenoid wound round the outside of the helium Dewar. This primary coil gave about 20 gauss per ampere and had additional compensating turns at the ends to ensure constancy of the magnetic field over the specimen volume to within .2%. This coil was driven by an audio oscillator and the value of the magnetic field was calculated from current readings. The signal from the secondary coil was led to the top of the cryostat by coaxial cable and fed to an amplifier which could be fitted with narrow band-pass filters. The output of the amplifier was read on an RMS vacuum tube voltmeter.

The electromotive force (e.m.f.) induced in the secondary coil depends on the state of the specimen which forms the core. In the normal state the flux linked is that due to the oscillating field diminished only by the diamagnetic influence of the eddy currents induced in the specimen. In the purely superconducting case the flux linked should be very close to zero but a small contribution remains due to leakage of flux through the small space between the coil and the specimen and through the penetration depth of the magnetic field into the specimen. The main difficulty with this method is that, with a specimen of high purity, the flux linked in the normal case may be so diminished by eddy current shielding that the change over the superconducting transition may be quite small.

The conditions in the intermediate state are much more complicated. Since these intermediate state effects influence the transition which is observed by this technique, and since the method is being used not merely to detect superconductivity but to study the transition itself, it is interesting to analyze this situation in order to know precisely what is being measured during the transition. The process is, in the general case, one of repeated magnetization in the superconducting state, passage through the intermediate state, and destruction of superconductivity in alternate directions. This is illustrated in Fig. 1 in which the peak value of the external field is shown in relation to a portion of the H_c–T diagram of the specimen. As the external field varies in time during one cycle from the point A the specimen remains superconducting until a certain fraction of the value of the critical field at that temperature is reached at B. From B until the full value of H_c is reached the specimen is in the intermediate state after which it is fully normal until the value H_c is reached again with diminishing external field. During this whole process there has been a certain value of $\partial B/\partial t$ giving the signal which is observed. The observed transition then consists of the variation of the fundamental component of $\partial B/\partial t$ as the temperature is lowered from T_c until at C the peak external field H_e is no longer able to generate the intermediate state.

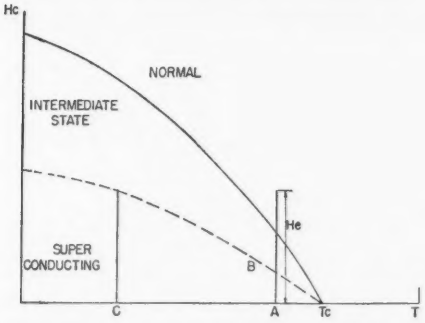

FIG. 1. Comparison of the applied oscillating magnetic field with the critical field curve.

The values of B and $\partial B/\partial t$ can be calculated for any portion of this transition region if the magnetization during the superconducting and intermediate states is known. Shoenberg (1937) has measured the magnetization of a cylinder of length:diameter ratio unity in a longitudinal magnetic field through the superconducting and intermediate states. In the case of a non-ideally shaped body the magnetization phenomena are complex and largely governed by the behavior of trapped flux. These effects depend considerably on the shape and condition of the specimen but it is still of interest to use Shoenberg's magnetization curves in comparison with the present results even if the cylinders are of different ratios.

Shoenberg's curves of intensity of magnetization can be replotted to give B as a function of H and differentiation gives the required variation of $\partial B/\partial t$ with external field. The form of these curves depends on the relative values of the peak external field H_e and the field required to initiate the intermediate state. Two of them, of one complete cycle, for $H_e=5H_c$ and for $H_e=H_c$ are given in Fig. 2. In Fig. 3 are pictures taken on an oscilloscope of the amplified

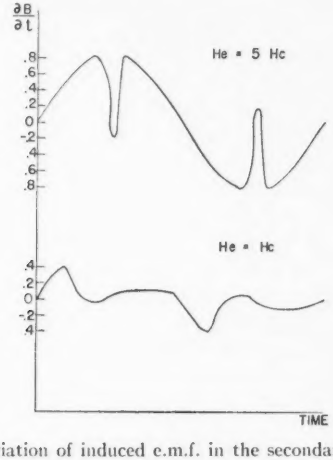

FIG. 2. Predicted variation of induced e.m.f. in the secondary coil at two temperatures during the transition.

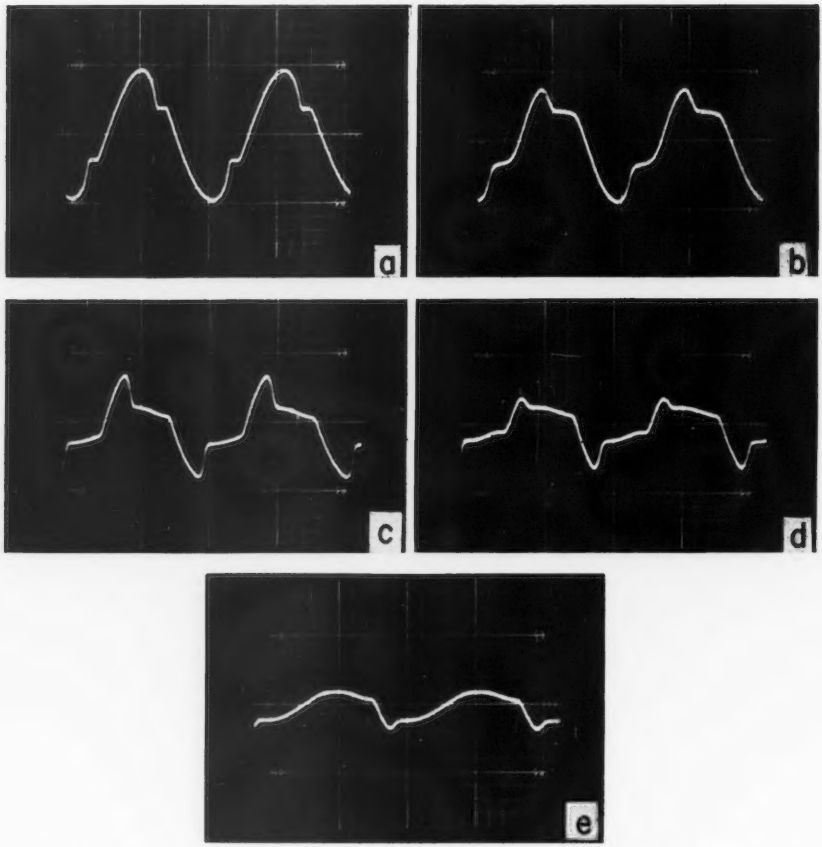

FIG. 3. Oscillograms of the secondary coil output during the transition. They are numbered in order of decreasing temperature. Frequency 1000 cycles/second. $H_e = 2$ gauss.

output from the secondary coil (without filters). They were taken at intervals through the transition from a point just after the transition had started until just before the signal becomes its residual constant value and so represent the output for various values of the ratio H_e/H_c. These observations were made on the largest grain-size specimen using a comparatively large oscillating field, about 2 gauss, so as to illustrate the intermediate state properties. The predicted curves in Fig. 2 should be compared with pictures *a* and *d* of Fig. 3 which refer approximately to the ratios quoted. Two points of interest arise. The first is that, as anticipated, the trapped flux region which dominates the $H_e = H_c$ curve is only approximately represented by the predicted curve. One of the possible contributions to this discrepancy is suggested by the second feature of the curves which is exhibited in the curve for $H_e = 5H_c$. The predicted

curve for this ratio has a distorted region arising from the passage through the superconducting and intermediate state regions when the external field is passing through the region near zero, i.e., $\partial B/\partial t$ is a maximum. However, the observed curve shows a kink displaced from the maximum of the e.m.f. This can presumably be ascribed to lagging of the flux changes arising from finite phase boundary velocities. This is supported by comparison of the present observations at a frequency of 1000 cycles per second and the similar oscillograms shown by Galkin and Bezuglyi (1955) for a frequency of 200 cycles per second where the displacement is less. The signal which was measured during the transition is the fundamental component of the curves of $\partial B/\partial t$ but no attempt has been made to analyze the curves for comparison with the measured signals. This is the nature of the transition which is observed by this method and if it is to be used to study the superconducting transition itself and measure transition widths there is the obvious necessity to work with the smallest possible values of H_e. In the present work values of H_e down to 0.1 gauss could be used and this would correspond to an intermediate state width of only .7 millidegrees, which is small compared with the observed transition widths of about 20 to 70 millidegrees. Confirmation that this instrumental transition width is not influencing the observed transition widths comes from observation of the transition with various values of H_e. It is found that the observed transition width can be reduced by reducing the value of H_e only to a certain point. Thereafter the transition width is independent of the primary field and all results illustrated refer to this limiting condition. In any case, no attempt to provide shielding from the earth's magnetic field was made and this could account for a transition width of about 3 millidegrees. Even this, however, is not a serious factor in the case of the small crystal specimen although it presumably does contribute more significantly to the transition for the largest grain-size specimen.

PROCEDURE

The transitions were studied by measuring the output of the secondary coil while slowly reducing the temperature. The pressure was read on a mercury manometer which measured absolute pressures and which could be read to 1/10 mm. Corrections to the temperature for hydrostatic pressure head of helium above the specimen were made and temperatures were calculated using the $T55_e$ temperature scale (Clement *et al.* 1955). The transitions were repeated over a range of values of H_e and for the two frequencies of 400 and 1000 cycles per second.

RESULTS

The transition curves for the various grain sizes are shown in Fig. 4. The quantity plotted vertically is the secondary coil output normalized so that the drop in signal over the transition is from unity to zero. Using this normalization no dependence of the transition on frequency could be detected and all the curves refer to values of the peak external field ($\sim 10^{-1}$ gauss) low enough to be negligible in affecting the transition width. The curves are composed of

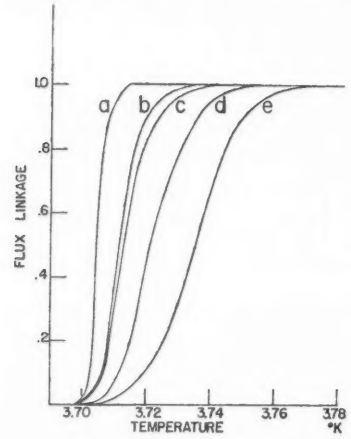

FIG. 4. Transitions for the various grain sizes. The average grain sizes are, reading from left to right: (*a*) approximately single crystals; (*b*) 5.5 mm; (*c*) 3.0 mm; (*d*) 1.4 mm; (*e*) 0.2 mm.

numbers of points ranging from 26 for the sharpest transition to about 100 for the widest obtained from repeated runs. The scatter of the points is never more than a total range of 4 millidegrees in temperature and .04 in susceptibility. These extreme values are exceptional and the normal scatter is about half the value quoted. The influence on the transition of the grain-size width is illus-

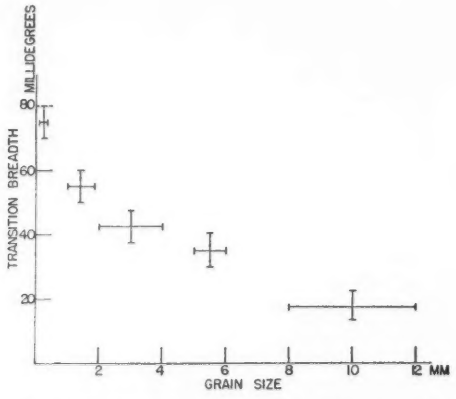

FIG. 5. Dependence of total transition width on grain size.

trated in Fig. 5. In this the transition width is the total width of the transition from the point at which the onset could just be detected to the point at which the induced e.m.f. had just become constant (both detectable to about one part in one thousand of the total change). The uncertainties in transition width are

estimated from the scatter of the measured points on the curves and the uncertainties in grain size from the observed range in diameters. The specimen which was almost a single crystal is difficult to define in this way and the value quoted for the mean grain size is an estimate of the range of single crystal current path for the circumferential currents induced by the experimental procedure.

Another specimen which was much more nearly a single crystal (containing only a small amount of striation substructure) gave a total transition breadth of only 3 millidegrees. However, it came from a different batch of material and is not quoted as part of the series illustrating the influence of grain boundaries alone.

DISCUSSION

The general result of the experiment is to confirm the original observation of de Haas and Voogd that the influence of grain boundaries is to broaden the transition only in the direction of increasing temperature away from a fairly well-defined vanishing point of resistance. Although it is not visible on the scale of Fig. 4 all the curves reach the superconducting state within about 2 millidegrees between 3.697 and 3.699° K. The broadest transition reported by de Haas and Voogd for a wire covers about 60 millidegrees, while the broadest one presently reported for a bulk specimen is about 75 millidegrees. This last is probably close to a limiting value as the specimen had about the smallest grain size which can be obtained in pure tin.

For a single crystal Webber, McGuire, and Reynolds report a transition breadth of 20 millidegrees and this can be compared with the value of 18 millidegrees for the largest grain size of the series. As stated above, a specimen freed from the last traces of large angle boundaries and most of the striation substructure gave a total width of about 3 millidegrees so that the first introduction of misorientation has a relatively large effect on the transition breadth.

The problem is thus to explain the nature of the partial superconductivity observed above the bulk transition temperature. It is not yet possible to say whether this is an effect taking place at the grain boundaries themselves or whether it can arise from thermal contraction mismatch between areas of crystal misorientation. For an ideal case of misorientation Faber (1957) has evaluated the transition temperature shift in tin to be of the order of 100 millidegrees upwards. This certainly covers the observed magnitude of the effect but the extension of the treatment to the genuinely polycrystalline case is not easy.

REFERENCES

CLEMENT, J. R., LOGAN, J. K., and GAFFNEY, J. 1955. Phys. Rev. **100**, 743.
FABER, T. E. 1957. Proc. Roy. Soc. A, **241**, 531.
DE HAAS, W. J. and VOOGD, J. 1931. Leiden Communication, 214*c*.
GALKIN, A. A. and BEZUGLYI, P.A. 1955. Soviet Phys. **1**, 197.
SHOENBERG, D. 1937. Proc. Camb. Phil. Soc. **33**, 260.
WEBBER, R. T., REYNOLDS, J. M., and MCGUIRE, T. R. 1949. Phys. Rev. **76**, 293.

ON THE SPHERICAL OSCILLATOR NUCLEUS[1]

T. D. NEWTON

ABSTRACT

The degree of consistency of an oscillator model of a nucleus is examined by means of a type of Hartree–Fock calculation based on a simple form of internucleon potential valid at low energies. An effective mass equal to 0.757 times the mass of a free nucleon is used. The oscillator wave functions are found to be not far from self-consistent and the oscillator frequency derived is physically reasonable, but the bound on the binding energy is not good. It is also shown that the oscillator wave functions are a good approximation for the state functions of particles bound in a finite potential well having the shape of a cutoff oscillator so that the Hartree–Fock calculation can be used to prescribe a shell model potential.

SECTION 1. THE PROBLEM

Frequently in problems of nuclear physics it is necessary to assume some radial wave function to represent the motion of a single nucleon in a nucleus. For such cases an oscillator function is often chosen (e.g. Talmi 1952; Tauber and Wu 1957) principally because its properties are well known and its analytic behavior is relatively simple. In these cases one is concerned to obtain an estimate of some matrix element and is not committed to any statement about the potential in which the nucleons move.

However, there have been several more detailed studies in which properties of physical nuclei have been related to an oscillator shell model. The earliest shell model level orderings obtained with j–j coupling (Mayer 1949; Haxel, Jensen, and Suess 1949) used that model. More recently Nilsson (1955) has made extensive calculations of levels in spheroidal oscillator wells and these have been used in combination with the collective model of Bohr and Mottelson (1953) for the prediction of spins and parities of nuclear ground states (Mottelson and Nilsson 1955) and for quite detailed comparison with excited states of light nuclei (for example Litherland, Paul, Bartholomew, and Gove 1956), but there is not, in the literature, any real justification for the use of oscillator wave functions for nucleons in nuclei.

We shall try to show that there is, in fact, some justification for using the oscillator form as the central potential of a single-particle model of a nucleus. The method is to determine, in as quantitative a fashion as seems easily possible, the departure of the oscillator potential from self-consistency in a Hartree–Fock calculation using a simple non-singular internucleon potential (equation 17) which correctly describes the two-nucleon interaction at low energies, i.e. it yields the description of the deuteron and various of its interactions (Feshbach and Schwinger 1951) and fits the low-energy proton–proton differential scattering cross section (Hall and Powell 1953).

[1]Manuscript received February 16, 1959.
Contribution from the Theoretical Physics Branch, Atomic Energy of Canada Limited, Chalk River, Ontario.
Issued as A.E.C.L. No. 845.

Our purpose is modest; such a calculation can not be expected correctly to determine, for example, the binding energy of nuclei or the true density of nuclear matter. This requires much more refined methods, including the correlation of nucleon motions and the proper description of high-energy interactions within the nucleus. The Hartree–Fock procedure is not applicable to the singular potentials computed by Gammel and Thaler (1957) and it would be very difficult to apply it to the complicated potentials of Signell and Marshak (1958).

On the other hand, for an examination of the most suitable wave functions to use in the unperturbed shell model one may be permitted to use simple methods and a potential fitted only at low energies. Previous calculations of this general nature have been made by Rotenberg (1955) and by Talman (1956). Both of these calculations started with the wave functions of a square well and then improved the function and potential by interaction. In both cases, but particularly in Talman's calculation, the resultant potential appears, superficially at least, more like a cutoff oscillator than like the original square well.

The calculation presented in Section 3 was designed to examine the usefulness of the oscillator functions as an initial approximation and to see what results can be obtained in that approximation by the use of a momentum-dependent shell model potential, i.e. an effective mass less than unity for a nucleon in a nucleus (Brueckner and Gammel 1958). The calculation does not contain an iterative process. Instead we have computed matrix elements between single-particle-occupied states of the Hartree–Fock Hamiltonian operator, taking exchange completely into account. These elements can then be compared directly with the corresponding elements of the single-particle Hamiltonian. The comparison shows qualitatively that the oscillator wave functions are nearly self-consistent. No absolute result is obtained, because the nature of the calculation does not justify the time and expense of attempting the self-consistency calculation.

However, one does obtain an explicit statement, in a known unperturbed oscillator shell model, of the energy level scheme appropriate to an internucleon potential valid at nuclear energies. This was not provided by the two earlier computations and it may be interesting to compare it with the calculations of binding in a finite nucleus. After the work reported here was completed Brueckner (1959) announced a self-consistent calculation of Ca^{40} using the effective two-body potential derived from his treatment of infinite nuclear matter. The comparison of his results with ours gives an indication of the effect of properly treating the high-energy interactions.

It is clear that any reasonable shell model potential must go to zero outside the nucleus. Therefore we first establish (in Section 2) that the bound eigenvalues and eigenfunctions of a "cutoff oscillator" potential are negligibly different from those of the corresponding states of a complete oscillator. Once this result is established we will use simple oscillator functions since only bound states are treated in this paper.

SECTION 2. THE CUTOFF OSCILLATOR POTENTIAL

As a preliminary, we will here examine the single-particle bound state wave functions which satisfy the Schrödinger equation

$$\{-(2M)^{-1}\hbar^2\nabla^2+V(r,\theta,\phi,\zeta,p^2)\}\psi = E\psi. \tag{1}$$

$$V = -V_0+\tfrac{1}{2}\mu^*\omega^2r^2+C\,l.s+D.l^2+\hbar^2(M^{-1}-M^{*-1})\nabla^2 \qquad \text{in } r < R_v \tag{2a}$$

$$V = 0 \qquad \text{in } r \geqslant R_v \tag{2b}$$

$$R_v = (2\mu^{*-1}\omega^{-2}V_0)^{1/2} \tag{2c}$$

$$\mu^* = (2M/M^*-1)^{-1}M. \tag{2d}$$

In (2) M represents the true mass of a nucleon and M^* the effective mass defined according to the present custom in nuclear physics, i.e. so that the approximation to the true total Hamiltonian given by $\sum_i (T_i+\frac{1}{2}V_i)$ shall contain a momentum-dependent term

$$(2M)^{-1}\sum_i p_i^2-\tfrac{1}{2}(M^{-1}-M^{*-1})\sum_i p_i^2 = (2M^*)^{-1}\sum_i p_i^2.$$

The mass parameter for the single-particle wave equations then becomes μ^* defined in (2d). C and D are coupling constants as used by Nilsson (1955).

If we put

$$y = \alpha r^2, \qquad \alpha = \mu^*\omega/\hbar \tag{3a}$$

the solution of (1) in the region $y < \alpha R_v^2$ is

$$\psi = r^l \exp(-y/2)F(y)X_{ljm}(\theta,\phi,\zeta). \tag{3b}$$

X_{ljm} is a function of spin and angle variables with the properties indicated by the subscripts;

$$X_{ljm} = \sum_\nu (l, \tfrac{1}{2}, m-\nu, \nu|jm)\,Y_l^{m-\nu}(\theta\phi)\,\chi_{\frac{1}{2}}^\nu(\zeta). \tag{4}$$

In (4) the bracket representation is used for the Clebsch–Gordan coefficients; $Y_l^{m-\nu}$ is a normalized spherical function and $\chi_{\frac{1}{2}}^\nu$ a spin function. The differential equation for $F(y)$ is

$$y\frac{d^2F}{dy^2}+(l+3/2-y)\frac{dF}{dy}-aF = 0, \tag{5a}$$

where

$$E+V_0 = (-2a+l+3/2)\hbar\omega+C\lambda_j+Dl(l+1) \tag{5b}$$

$$\begin{aligned} \lambda_j &= \tfrac{1}{2}l && \text{if } j = l+\tfrac{1}{2} \\ &= -\tfrac{1}{2}(l+1) && \text{if } j = l-\tfrac{1}{2}. \end{aligned} \tag{5c}$$

The solution of (5a), which is well behaved at $y = 0$, is the confluent hypergeometric function

$$F(y) = \Phi(a, c; y) \tag{6}$$

in the notation of Bateman (1953, Vol. 1, p. 248). Thus the bound states of equation (1) are

$$\psi = C_{al} r^l \exp(-\alpha r^2/2) \Phi(a, l+3/2; \alpha r^2) X_{ljm}(\theta, \phi, \zeta) \qquad \text{in } r < R_v \tag{7a}$$

$$= C_{\kappa l} r^{-\frac{1}{2}} K_{l+\frac{1}{2}}(\kappa r) X_{ljm}(\theta, \phi, \zeta) \qquad \text{in } r > R_v. \tag{7b}$$

In (7b) $K_{l+\frac{1}{2}}$ is that Bessel function of imaginary argument defined by Watson (1952) which decays exponentially for large κr, and

$$\kappa = \hbar^{-1}\sqrt{(2M|E|)}. \tag{7c}$$

C_{al} and $C_{\kappa l}$ are normalizing constants.

The energy eigenvalues of the bound states are determined by the requirement that the logarithmic derivative of ψ be continuous at $r = R_v$. This condition, in terms of $Y = \alpha R_v^2$, may be written

$$\Phi^{-1}\Phi' = \tfrac{1}{2} + (2Y)^{-1}\{\kappa R_v (K_{l+\frac{1}{2}})^{-1}(K_{l+\frac{1}{2}})' - l - \tfrac{1}{2}\}, \tag{8}$$

where all functions are evaluated at $y = Y$, ($r = R_v$) and the prime represents differentiation with respect to the argument of the function to which it is attached.

If we define

$$E = -\nu\hbar\omega \tag{9}$$

so that

$$\kappa^2 R^2 = -2\hbar^{-2} M E R^2 = 2\nu Y M/\mu^*,$$

and if we define also

$$S_l = \kappa R_v (K_{l+\frac{1}{2}})^{-1}(K_{l+\frac{1}{2}})' - l - \tfrac{1}{2} \tag{10}$$

then the term on the left of (8) may be evaluated as a function of ν, Y, from the recursive relation

$$S_0(\nu, Y) = -\{1 + \sqrt{(2\nu Y M/\mu^*)}\} \tag{11a}$$

$$S_l(\nu, Y) = -(2l+1) + 2(\nu Y M/\mu^*)/S_{l-1}. \tag{11b}$$

Finally there is the relation (Bateman 1953, Vol. 1, p. 254)

$$\frac{d}{dx}\Phi(a, c; x) = c^{-1} a \Phi(a+1, c+1; x)$$

so that (8) becomes an equation for ν,—

$$a\Phi(a+1, l+5/2; Y) - \tfrac{1}{4}(2l+3)\{1 + Y^{-1} S_l(\nu, Y)\}\Phi(a, l+3/2; Y) = 0 \tag{12a}$$

$$2a = \nu + \tfrac{1}{2}(2l+3-Y) + \{C\lambda j + Dl(l+1)\}/\hbar\omega. \tag{12b}$$

For given Y, M/μ^*, C, and D each solution $\nu > 0$ of (12) defines the radial factor of a set (various l, j, m) of bound state functions of a single particle in the potential (2). As Y is increased the values of $E + V_0 - C\lambda j - Dl(l+1)$ approach $(N+3/2)\hbar\omega$, i.e. the energy eigenvalues of an isotropic oscillator;

in terms of the parameters of (12*b*) a tends toward a negative integer, $-n$. Hence the effect of the cutoff may be represented by the value of $\epsilon = n+a$ and also by the energy shift.

Table I displays the parameters which define bound states in a cutoff oscillator well when $\mu^*/M = 0.6089$ and for the indicated values of C and D.

TABLE I

Bound energy levels of the cutoff oscillator potential of equation (2) with $\mu^*/M = 0.6089$; $V_0 = 5.7798\hbar\omega$. $a = -n+\epsilon$. $-2\epsilon\hbar\omega$ is the increase of the energy of the cutoff oscillator over that of the complete oscillator

$C = 0$, $D = 0$				$C = -0.1\hbar\omega$, $D = -0.0225\hbar\omega$				
l	n	$-\epsilon$	$-E/\hbar\omega$	l	j	n	$-\epsilon$	$-E/\hbar\omega$
0	0	.0001	4.2796	0	1/2	0	.0001	4.2796
1	0	.0006	3.2786	1	3/2	0	.0006	3.3735
2	0	.0023	2.2752	1	1/2	0	.0006	3.2236
0	1	.0044	2.2710	2	5/2	0	.0026	2.5097
3	0	.0048	1.2702	0	1/2	1	.0044	2.2710
1	1	.0105	1.2588	2	3/2	0	.0022	2.2602
0	2	−.0102	.3003	3	7/2	0	.0067	1.6863
2	1	−.0069	.2937	1	3/2	1	.0116	1.3517
4	0	−.0022	.2842	3	5/2	0	.0052	1.3394
				1	1/2	1	.0098	1.2052
				4	9/2	0	.0122	0.9054
				2	5/2	1	.0092	0.4965
				4	7/2	0	.0036	.4725
				0	1/2	2	−.0102	.3003
				5	11/2	0	.0085	.1878

The parameters μ^*/M, V_0, and R_c have been chosen so that comparisons can be made with the Hartree–Fock values of Section 3. For simplicity D has been given the same value for all shells. This case is completely typical; it is unnecessary to give tables for other values of $V_0/\hbar\omega$.

It may be seen that there is a remarkably small change of energy due to cutting off the oscillator potential, and this result is not modified by the presence of terms $Cl.s+Dl^2$. Even levels lying very near the top of the well are but slightly changed. The potential (2) would be appropriate for the neutrons in a model nucleus. The proton potential should include a Coulomb barrier and so the shifts of proton levels would be even smaller than those shown in Table I.

It is interesting to observe that the direction of the energy shift varies with the magnitude of μ^*/M. It is easily seen that when $\mu^*/M = 1$, all bound levels are lowered in energy, but as μ^*/M decreases one finds that some levels are raised. This is caused, of course, by the changed condition on the slope of the radial function at $r = R_c$. If the logarithmic derivative imposed by the Hankel function of the external region is smaller in magnitude than that of the original oscillator function, the energy of the state is decreased, and vice versa. Since the effective mass ratio is unity outside the nucleus the imposed slope is independent of μ^*, while the slope of the oscillator function depends on the effective mass used in the internal region.

Not only are the bound energy levels very nearly undisturbed by the cutoff,

but also the wave functions are very little changed. This may be demonstrated by comparing the positions of the nodes of the wave functions of the cutoff and complete oscillator potentials, i.e. we have to consider the roots of

$$\Phi(-n+\epsilon, l+3/2; y) = \sum_{k=0}^{\infty} \frac{(-n+\epsilon)_k}{(l+3/2)_k} \frac{y^k}{k!} = 0 \tag{13}$$

as functions of ϵ. Here $(c)_0 = 1$, $(c)_k = c(c+1)-(c+k-1)$. Since $l+3/2 > 0$, this equation has just n real positive roots when $0 \leqslant \epsilon < 1$ (Bateman 1953, p. 288).

This study can be aided by consideration of the polynomials

$$p_n(\epsilon, c; x) = \sum_{k=0}^{n} \frac{(-n+\epsilon)_k}{(c)_k} \frac{x^k}{k!}$$

and

$$q_n(\epsilon_1, \epsilon_2, c; x) = \sum_{k=0}^{n} \frac{(-n+\epsilon_1)_k}{(c)_k} \left(\frac{1-\epsilon_2}{1-\epsilon_1}\right)^k \frac{x^k}{k!}.$$

If $1 > \epsilon_2 > \epsilon_1 \geqslant 0$ it is clear that the value of each term of $p_n(\epsilon_2)$ lies between the values of the corresponding terms of $p_n(\epsilon_1)$ and $q_n(\epsilon_1\epsilon_2)$. Consequently the values of the polynomials are similarly intermediate, and so also are the positions of the roots. Thus if $x_k(n, \epsilon)$ denote the kth root of $p_n(\epsilon, c; x) = 0$,

$$x_k(n, \epsilon_1) \leqslant x_k(n, \epsilon_2) \leqslant \left(\frac{1-\epsilon_1}{1-\epsilon_2}\right) x_k(n, \epsilon_1) \qquad \text{if } 1 > \epsilon_2 > \epsilon_1 \geqslant 0. \tag{14a}$$

Now the difference

$$\Phi(-n+\epsilon, c; y) - p_n(\epsilon, c, y) = (-)^n \epsilon f_n(\epsilon, c, y)$$

vanishes at $\epsilon = 0$ and increases monotonically with $\epsilon > 0$ and $y > 0$. If $y_k(n, \epsilon)$ denote the kth root of (13), then

$$\begin{aligned} y_{n-2k}(n, \epsilon) &\leqslant x_{n-2k}(n, \epsilon) \\ y_{n-2k-1}(n, \epsilon) &\geqslant x_{n-2k-1}(n, \epsilon). \end{aligned} \tag{14b}$$

The equality sign holds in (14b) when $\epsilon = 0$, so that from (14a) and (14b) we have

$$(1-\epsilon) y_{n-2k}(n, \epsilon) \leqslant y_{n-2k}(n, 0) \tag{15a}$$

$$(1-\epsilon) y_{n-2k-1}(n, 0) \leqslant y_{n-2k-1}(n, \epsilon). \tag{15b}$$

When ϵ becomes unity $y_n(n, 1)$ becomes infinite, i.e. it coalesces with the singularity of Φ at infinity, while

$$y_j(n, 1) = y_j(n-1, 0) \qquad \text{for } j \leqslant n-1.$$

From (15) we see that

$$\frac{y_k(n, \epsilon) - y_k(n, 0)}{y_k(n, 0)} = (-)^{n-k}\epsilon + \text{terms in higher powers of } \epsilon. \tag{16}$$

Thus, although this discussion has been limited to positive values of ϵ, the analyticity in a of $\Phi(a, c; y)$ requires that (16) hold also for ϵ near zero but negative and $k \leqslant n$. When $-1 < \epsilon < 0$, $\Phi(-n+\epsilon, c; y)$ has $n+1$ real roots, while there are just n roots $y_k(n, 0)$. In this case $y_{n+1}(n, 0)$ represents infinity and relation (16) does not follow from (15) for $k = n + 1$. This root, however, lies in the region $y > \alpha R_v^2$ and is not a node of our wave functions if ϵ is sufficiently small.

For the values of ϵ shown in Table I, we see that the radial zeros of ψ are shifted by about 0.5% (about 1% change in αr^2) from the zeros of the complete oscillator functions. The principal difference between the functions (7) and oscillator functions occurs in the region $r \geqslant R_v$; ψ of (7) describes a "softer" surface, but the distribution of particles within the nucleus is very little different from the distribution defined by oscillator functions.

SECTION 3. AN HARTREE–FOCK CALCULATION

In this section we describe an Hartree–Fock (denoted H.F. in sequel) calculation of the ground state of a model nucleus. We assume a nuclear wave function constructed from one-particle oscillator functions. In the last section we have learned that these are negligibly different from the corresponding single-particle states in a cutoff oscillator potential, so that they form a reasonable basis for the calculation. Moreover, it is well known that a nuclear model based on these functions displays many of the properties of a physical nucleus, particularly when combined with the collective motions of the theory of Bohr and Mottelson (1953) or when treated by the methods of Elliott (1958).

We will compute the matrix elements between occupied levels of the H.F. Hamiltonian, derived from the Serber–Yukawa two-body potential,

$$V(r) = (1+P_M)J(r) \tag{17a}$$

$$J(r) = \tfrac{1}{2}Ce^2r^{-1}\exp(-\mu r) \tag{17b}$$

$$C = -40; \qquad \mu = 2.5\, mc^2/e^2. \tag{17c}$$

In (17) P_M is the Majorana operator which exchanges position co-ordinates. The constants are those used by Lane, Thomas, and Wigner (1955).

The potential (17) is not a suitable nuclear potential at all energies. Recent high-energy proton–proton and neutron–proton scattering experiments have best been described by an internucleon potential containing a repulsive core and a much more complicated form outside the core. A non-integrable core (Gammel and Thaler 1957) in a normal Hartree–Fock type of calculation leads to divergences, and the potential of Signell and Marshak (1958) is too complicated for easy analysis.

One can give a qualitative argument for using in an H.F. calculation the simple form (17) together with a momentum dependence; the basis of the argument is that the true potential is first replaced by a pseudo potential, and the latter used for the H.F. process. Pseudo potentials have been computed as point operators (Huang and Yang 1957; Lee, Huang, and Yang 1957) for

hard spheres, but a different kind of pseudo potential can be imagined. For unbound spinless particles, the specification of all phase shifts as a function of energy is equivalent to the specification of a two-body potential; so to match the effect of a given potential on all unbound particle motions, it suffices to match all asymptotic phase shifts. If, in addition, the given potential vanishes on, or can be exactly treated outside, some surface it suffices to match the phase shifts on that surface. This may be done either by specifying a boundary condition there, or by specifying some other momentum-dependent pseudo potential within the boundary which will produce the same set of phase shifts. An example of such a pseudo potential for a very simple original potential is given in an appendix to this paper.

This computation would become more complicated if it were attempted for the recent internucleon potentials. The presence of tensor and spin–orbit forces requires the matching of scattering matrices instead of simple phase shifts, and the choice of a suitable boundary surface is not easy. We do not here intend to attempt such a calculation; the concept is introduced merely to point out that a computation with the simple form (17) is not wholly without sense. That form, combined with a tensor term, was proposed by Feshbach and Schwinger (1951), and fitted to the low-energy data of the two-nucleon system. Hall and Powell (1953) fitted their proton–proton scattering data up to 4 Mev using the same form and determining the remaining free parameters. Thus the Feshbach–Schwinger potential, of which (17) is the central part, may be regarded as an experimentally determined pseudo potential valid at low energies. The tensor part of the Feshbach–Schwinger potential would make no contribution to the energy of a system with saturated spins, so that in the filled shell systems which we discuss its effect would always be small, i.e. it would have a (small) effect only on the states of an incomplete l-shell. Hence it is legitimate in our calculation to use only the central term, i.e. equation (17).

The concept of pseudo potential outlined above is not very different in principle from the more elegant and more rigorous concepts of Brueckner's theory (see for example Bethe 1956; Gomes, Walecka, and Weisskopf 1958). That theory has been used to show that in infinite nuclear matter a complex internucleon potential is approximately equivalent to a one-body potential which includes a term proportional to k^2 (Brueckner and Gammel 1958).

We shall not here attempt to justify the use of any particular value of the momentum dependence of the one-body potential. The fact that an effective mass less than unity should be used in a shell model of a nucleus is by now well established; a method which, in principle, should permit it to be calculated within the framework of the Hartree–Fock process has been proposed. We treat the ratio μ^*/M (cf. equation 2) as a parameter of the computation.

It remains briefly to describe the computation of the H.F. potential matrix. We shall calculate it only for systems in which both neutrons and protons form closed j–j coupled angular momentum shells. The trial wave function for the system of particles is then a Slater determinant composed from single-particle wave functions,

$$\psi_{n\,l\,jm\tau} = R_{n\,l}(r)X_{l\,jm}(\theta, \phi, \zeta)\Omega(\tau), \tag{18}$$

where

$$R_{n\,l} = C_{n\,l}\, r^{\,l} \exp(-\alpha r^2/2)\, L_n^{l+\frac{1}{2}}(\alpha r^2)$$

$$\alpha = \mu^* \omega \hbar^{-1}$$

$$C_{n\,l} = (2\alpha^{l+3/2} n!)^{\frac{1}{2}} / \sqrt{\{\Gamma(n+l+3/2)\}}.$$

The function (18) differs from (3*b*) in that we here use the wave functions of the complete, not the cutoff, oscillator and (18) also includes a function $\Omega(\tau)$ of the isotopic spin in order that the total nuclear wave function may be written as a single Slater determinant. Since the potential (17) is charge independent, $\Omega(\tau)$ is a simple two-valued function. $L_n^{l+\frac{1}{2}}$ is a generalized Laguerre polynomial in the notation of Bateman (1953, Vol. 2, p. 188). The function $X_{l\,jm}$ of angle and spin has been defined in Section 2. The *j*–*j* coupling is imposed, say, by the Nilsson (1955) coefficients, but this is not significant for our H.F. calculation. The justification of the spin–orbit coupling term in shell theory is an unsolved problem of long standing to which the present calculations make no contribution; since we limit ourselves to closed shell systems only the radial dependence of the central potential can be discussed.

Now let ξ stand for the five co-ordinates $(\mathbf{x}, \zeta, \tau)$ of one particle. We set up, and shall seek to minimize, the integral

$$\langle H-E\rangle = \int d\xi_1 \ldots d\xi_A \bar{\Psi}(\xi_1 \ldots \xi_A)\{\sum_i T_i + \sum_{ij} v(\xi_i, \xi_j) - E\}\Psi(\xi_1 \ldots \xi_A) \tag{19}$$

in which Ψ represents the Slater determinant formed for N neutrons and Z protons $(N+Z = A)$ from the single-particle functions (18). T_i is the ith kinetic energy operator and the two-body potential $v(\xi_i, \xi_j)$ is that defined by (17). The integral includes 3*A*-fold spatial integration and sums over all spin and isotopic spin variables. The reduction of (19) when spin and orbital angular momentum are uncoupled is obvious; essentially the same reduction is possible for our *j*–*j* coupled wave functions. The results are particularly simple when $v(\xi_i, \xi_j)$ includes the Serber exchange mixture contained in (17). We note first that the potential terms of (19), after expansion of the (normalized) Slater determinants, use of the symmetry of the potential sum, summing over isotopic spin, and application of the exchange operator $(1+P_M)$ become

$$\langle V\rangle = \tfrac{1}{2} \sum_{\rho,\nu} \sum_{\zeta_1\zeta_2} \int d\mathbf{x}_1\, d\mathbf{x}_2 J(\mathbf{x}_1\mathbf{x}_2)\bar{\psi}_\rho(\mathbf{x}_1\zeta_1)\bar{\psi}_\nu(\mathbf{x}_2\zeta_2). \tag{20}$$

$$[\psi_\rho(\mathbf{x}_1\zeta_1)\psi_\nu(\mathbf{x}_2\zeta_2) + \psi_\rho(\mathbf{x}_2\zeta_1)\psi_\nu(\mathbf{x}_1\zeta_2)$$

$$-\delta_{\tau_\rho\tau_\nu}\{\psi_\rho(\mathbf{x}_1\zeta_2)\psi_\nu(\mathbf{x}_2\zeta_1) + \psi_\rho(\mathbf{x}_2\zeta_2)\psi_\nu(\mathbf{x}_1\zeta_1)\}].$$

In (20) $\mathbf{x}_i$ represents the three spatial co-ordinates of particle i, the states $\psi_\rho(\mathbf{x}_1\,\zeta_1)$ no longer contain the factor $\Omega(\tau)$, and the sums over ρ, ν extend over all occupied states. We now consider that part of the sums in (20), extending over one or two closed *j*–*j* shells, in which the radial part of the wave

function is constant. The angle and spin function X_{ljm} is written out in equation 4, Section (2). We have

$$(21)\qquad \sum_{\zeta,m} \bar{X}_{ljm}(\theta_i\phi_i\zeta)\, X_{ljm}(\theta_k\phi_k\zeta)$$
$$= \sum_{q+\mu=m} (l,\tfrac{1}{2};q,\mu|j,q+\mu)^2\, \bar{Y}_l^q(\theta_i\phi_i)\, Y_l^q(\theta_k,\phi_k)$$
$$= \sum_q (2l+1)^{-1}(2j+1)\, \bar{Y}_l^q(\theta_i,\phi_i)\, Y_l^q(\theta_k,\phi_k).$$

To obtain (21) we have used the normalization property and the symmetry under interchange of (jm) with (lq) of the Clebsch–Gordan coefficients. Equation (21) provides the means for reduction of the first two sums in (20). The other two sums arise only when the states ρ, ν are filled by nucleons of like charge. In the ground state it will generally be true that at least one of the pairs of shells $j_\rho = l_\rho \pm \frac{1}{2}$, or $j_\nu = l_\nu \pm \frac{1}{2}$ will be completely occupied by nucleons of the same kind. In that case the double sum can be simplified. Suppose $j = l+\frac{1}{2}$ and $j = l-\frac{1}{2}$ are both occupied (this procedure is also applicable if $l = 0$ when only one shell occurs); then

$$(22)\qquad \sum_{\zeta_1\zeta_2}\sum_{jmm'} \bar{X}_{ljm}(\theta_1\phi_1\zeta_1)\, \bar{X}_{l'j'm'}(\theta_2\phi_2\zeta_2)\, X_{ljm}(\theta_i\phi_i\zeta_2) X_{l'j'm'}(\theta_k\phi_k\zeta_1)$$
$$= \sum_{qq'} (2l'+1)^{-1}(2j'+1)\, \bar{Y}_l^q(\theta_1\phi_1)\, Y_l^q(\theta_i\phi_i)\, \bar{Y}_{l'}^{q'}(\theta_2\phi_2)\, Y_{l'}^{q'}(\theta_k\phi_k).$$

Equation (22) follows from the ortho-normal properties of the Clebsch–Gordan coefficients. Since $(2l+1)^{-1}[\{2(l+\frac{1}{2})+1\}+\{2(l-\frac{1}{2})+1\}] = 2$, we may write, for the case when at least one of l, l' is completely filled, in analogy with (21)

$$(23)\qquad \sum_{\zeta_1\zeta_2}\sum_{mm'} \bar{X}_{ljm}(\theta_1\phi_1\zeta_1)\bar{X}_{l'j'm'}(\theta_2\phi_2\zeta_2)X_{ljm}(\theta_i\phi_i\zeta_2)X_{l'j'm'}(\theta_k\phi_k\zeta_1)$$
$$= \tfrac{1}{2}\sum_{qq'} \frac{(2j+1)}{(2l+1)}\frac{(2j'+1)}{(2l'+1)}\, \bar{Y}_l^q(\theta_1\phi_1)\bar{Y}_{l'}^{q'}(\theta_2\phi_2)\, Y_l^q(\theta_i\phi_i)\, Y_{l'}^{q'}(\theta_k\phi_k).$$

Note that (23) does not contain a sum over j.

We shall use (21) and (23) together with the addition law

$$(24)\qquad \sum_q \bar{Y}_l^q(\theta_i\phi_i)\, Y_l^q(\theta_k\phi_k) = (4\pi)^{-1}(2l+1)P_l(\cos\omega_{ik})$$

to simplify (20). If the system has two or more unpaired j shells (e.g. $j = l+\frac{1}{2}$ filled, $j = l-\frac{1}{2}$ unfilled, $l \neq 0$) containing nucleons of like charge, then (23) is an approximation for those particular shells.

Putting

$$(25)\qquad Z_{nlq}(\mathbf{x}) = R_{nl}(r)\, Y_l^q(\theta,\phi),$$

we have

$$(26)\qquad \langle H-E\rangle = \sum_\rho P_\rho \int d\mathbf{x}\, \bar{Z}_\rho\, (T_\rho - E_\rho)\, Z_\rho$$
$$+ \tfrac{1}{2}\sum_{\nu\rho} P_\rho P_\nu \int d\mathbf{x}_1 d\mathbf{x}_2 (1-\tfrac{1}{2}\delta_{\tau_\rho\tau_\nu}) J(\mathbf{x}_1\mathbf{x}_2)\bar{Z}_\rho(\mathbf{x}_1)\bar{Z}_\nu(\mathbf{x}_2)$$
$$\times\{Z_\rho(\mathbf{x}_1)Z_\nu(\mathbf{x}_2)+Z_\rho(\mathbf{x}_2)Z_\nu(\mathbf{x}_1)\}.$$

Except for the occupation numbers $P_\rho = (2l_\rho+1)^{-1}\,(2j_\rho+1)$, equation (26) is now the same as one would have obtained from a Slater determinant of functions with uncoupled spin and orbital angular momentum. This is the only remaining effect of the spin–orbit coupling and the matrix elements $\langle\rho|V|\nu\rangle$ between states Z_ρ, Z_ν are of course independent of the spin–orbit coupling constants used. The subscript ρ represents the triple quantum numbers $(n_\rho l_\rho q_\rho)$. The sum contains repeated terms for multiply occupied states.

The H.F.-linked system of equations is to be obtained by requiring that the integral (26) be stationary under variation of the single-particle wave functions $Z_{n\,lq}$. This is a standard procedure which leads to a system of equations

$$(27) \qquad (T-E_\rho)\,Z_\rho(\mathbf{x})+\sum_\nu V_{\rho\nu}(\mathbf{x})\,Z_\nu(\mathbf{x}) = 0.$$

Equation (27) can, in principle, be solved for $Z_\nu(\mathbf{x}_i)$. If the oscillator nucleus were self-consistent in the H.F. sense, the $Z_\nu(\mathbf{x}_i)$ which satisfy (27) would turn out to be just oscillator wave functions, and in the spherically symmetrical systems under study this solution is independent of the spin–orbit and orbital momentum dependence of the potential used to define the original ψ_{jlm} functions.

The direct terms of $V_{\rho\nu}(\mathbf{x})$ contain a factor $\delta_{\rho\nu}$ and can easily be compared as a function of r with the original oscillator potential. They indeed show an approximately quadratic dependence on r out to the nuclear boundary with a smoothed cutoff to zero potential energy there. The direct potential is, however, much shallower than the original oscillator form.

In order to obtain fairly simply a definite comparison between the complete H.F. equations (27) and the original single-particle equations, we have decided to compute the (single particle) matrix elements $\langle\nu|H|\rho\rangle$ of (27) and to see how they differ from the matrix elements of the original isotropic oscillator. This is a simpler calculation, and is more definite than the usual comparison of the average over ν of $V_{\rho\nu}(\mathbf{x})$ with the oscillator potential.

The matrix of the kinetic energy operator is well known, so we have only to compute the potential matrix whose elements are

$$(28) \quad \langle\nu|V|\rho\rangle = \sum_\sigma \int d\mathbf{x}\; Z_\nu(\mathbf{x})\; V_{\rho\sigma}(\mathbf{x})\; Z_\sigma(\mathbf{x})$$

$$= \sum_\sigma P_\sigma \int\!\!\int d\mathbf{x}_1\, d\mathbf{x}_2 (1-\tfrac{1}{2}\delta_{\tau_\rho\tau_\nu})\, J(\mathbf{x}_1\mathbf{x}_2)\bar{Z}_\nu(\mathbf{x}_1)\bar{Z}_\sigma(\mathbf{x}_2)$$

$$\times\{Z_\rho(\mathbf{x}_1)Z_\sigma(\mathbf{x}_2)+Z_\rho(\mathbf{x}_2)Z_\sigma(\mathbf{x}_1)\}.$$

Now the spatial dependence of the potential (17) may be written (Mott and Sneddon 1948, p. 387)

$$(29) \qquad J(\mathbf{x}_1\mathbf{x}_2) = \tfrac{1}{2}Ce^2\sum_\lambda (2\lambda+1)(r_1r_2)^{-\frac{1}{2}} I_{\lambda+\frac{1}{2}}(\mu r_a) K_{\lambda+\frac{1}{2}}(\mu r_b)\, P_\lambda(\cos\omega_{12})$$

in which $r_a < r_b$, and these are r_1, r_2 in some order; ω_{12} is the angle between $\mathbf{x}_1$ and $\mathbf{x}_2$, and $I_{\lambda+\frac{1}{2}}$, $K_{\lambda+\frac{1}{2}}$ are Bessel functions of imaginary argument as

defined by Watson (1952). When (29) is substituted in (28) we obtain the following sums of integrals over angle:

$$(30a)\quad \text{direct}\quad P_\sigma(2\lambda+1)\sum_{q\sigma}\int\!\!\int d\Omega_1 d\Omega_2 \bar{Y}^{q_\nu}_{l_\nu}(\theta_1\phi_1)\bar{Y}^{q_\sigma}_{l_\sigma}(\theta_2\phi_2)Y^{q_\rho}_{l_\rho}(\theta_1\phi_1) \times Y^{q_\sigma}_{l_\sigma}(\theta_2\phi_2)P_\lambda(\cos\omega_{12})$$
$$= P_\sigma(2\lambda+1)\,\delta_{\lambda 0}\delta_{l_\nu l_\rho}\delta_{q_\nu q_\rho}(2l_\sigma+1);$$

$$(30b)\quad \text{exchange}\quad P_\sigma(2\lambda+1)\sum_{q\sigma}\int\!\!\int d\Omega_1 d\Omega_2 \bar{Y}^{q_\nu}_{l_\nu}(\theta_1\phi_1)\bar{Y}^{q_\sigma}_{l_\sigma}(\theta_2\phi_2)Y^{q_\rho}_{l_\rho}(\theta_2\phi_2) \times Y^{q_\sigma}_{l_\sigma}(\theta_1\phi_1)P_\lambda(\cos\omega_{12})$$
$$= P_\sigma(2l_\sigma+1)(l_\sigma l_\rho 00|\lambda 0)^2\delta_{l_\nu l_\rho}\delta_{q_\nu q_\sigma}.$$

The matrix element (28) then reduces to a sum of integrals over the two radii, r_1 and r_2. We continue the separation into direct and exchange terms. Since $(2l_\sigma+1)P_\sigma = 2j_\sigma+1$ we have

$$(31a)\quad \langle\nu|V|\rho\rangle_D = \tfrac{1}{2}Ce^2\sum(2j_\sigma+1)\delta_{l_\nu l_\rho}(1-\tfrac{1}{4}\delta_{\tau_\rho\tau_\sigma}) \times\int\!\!\int r_1^{3/2}\,dr_1 r_2^{3/2}dr_2 I_{\frac{1}{2}}(\mu r_a)K_{\frac{1}{2}}(\mu r_b)\,R_\nu(r_1)R_\rho(r_1)\,R_\sigma^2(r_2),$$

$$(31b)\quad \langle\nu|V|\rho\rangle_E = \tfrac{1}{2}Ce^2\sum(2j_\sigma+1)(1-\tfrac{1}{2}\delta_{\tau_\rho\tau_\sigma})\delta_{l_\nu l_\rho}\sum_\lambda\,(l_\rho l_\sigma 00|\lambda 0)^2 \times\int\!\!\int r_1^{3/2}dr_1 r_2^{3/2}dr_2 I_{\lambda+\frac{1}{2}}(\mu r_a)K_{\lambda+\frac{1}{2}}(\mu r_b)R_\nu(r_1)R_\sigma(r_1)R_\rho(r_2)R_\sigma(r_2).$$

The integrals (31) are sums of Slater integrals of the form

$$(32)\qquad \int_0^\infty r_1^{k_1}\,dr_1\exp(-\alpha r_1^2-\mu r_1)\int_0^{r_1} r_2^{k_2}dr_2\,\frac{\sinh\mu r_2}{\mu}\exp(-\alpha r_2^2)$$

or those obtained by replacing $\sinh\mu r$ by $\cosh\mu r$.

The calculation of $\langle\nu|V|\rho\rangle$ was performed on the Chalk River datatron by evaluating integrals of form (32) for a sufficient range of values of k_1 and k_2, and then finding the combinations required for the sums (31). The Coulomb interaction between protons contains no Majorana operator so it is obtained from the same formulae by setting $\mu = 0$; replacing $\frac{1}{2}Ce^2$ by $-e^2$ in the direct term, and $+e^2$ in the exchange term; and limiting the sum to proton-occupied states. The integrals (32) were evaluated by direct numerical integration. This is relatively simple to do since they are essentially single integrals. The results were checked by comparison with analytic values in special cases and by recursion relations. For small values of k_1 and k_2 ($k_1 \sim 1$) the computed integrals were accurate to six significant figures; for larger values of k_1 this improved by about one figure. (Simple programs on the datatron are limited to eight figures.) Since these integrals have to be combined with varying coefficients and signs the final matrix elements are probably accurate to only

three or four figures, and in fact the exchange potential matrix elements involving $l = 4$ and $l = 5$ in Ba^{138} are only order of magnitude estimates. The machine values of these elements fluctuate widely with small changes of α, showing that significance of the result is almost completely lost.

SECTION 4. THE CHOICE OF PARAMETERS

In order to carry out the calculation of the matrices (31) it is necessary to specify the oscillator parameter $\alpha = \mu^*\omega/\hbar$; indeed one may choose different values α_N and α_P for the neutron and proton wave functions; they are parameters of the initial one-particle shell model wave functions, so we now consider that model.

The cutoff oscillator potential of Section 2 is defined by three parameters, the central depth V_0, the cutoff radius R_v, and the effective mass parameter μ^*. In any reasonable nuclear model based on this kind of potential we should expect that the central depth V_0 of the neutron potential is, in first approximation, the same in all nuclei, and that the cutoff radius is given by a form

$$R_v = a_v A^{1/3}. \tag{33}$$

It is not so clear that the momentum dependence of the potential as defined by the ratio μ^*/M should also be the same in all nuclei, but it is implied by the two previous assumptions and the systematics of nuclei. From the condition that the central potential for neutrons vanish at $r = R_v$ we obtain

$$\hbar\omega_N = \hbar\sqrt{(2V_0)}/(R_v\sqrt{\mu^*}). \tag{34}$$

The average binding of a neutron, given by the sum of the expectation values of the kinetic plus half the potential energies of the occupied states is, in a system containing N neutrons,

$$B_N = -\tfrac{1}{2}V_0 + (2N)^{-1}\sum_N{}'\{(1+\mu^*/2M)(2n+l+3/2) - 2\kappa\lambda_j - \kappa\mu l(l+1)\}\hbar\omega_N, \tag{35}$$

in which $(2n+l)$ is the number of the oscillator level, and the spin–orbit and angular momentum contributions are specified by $C = -2\kappa\hbar\omega$, $D = -2\kappa\mu\hbar\omega$ in the notation of Nilsson (1955). The sum $\sum_N{}'$ runs over all neutron-occupied states. We have shown that we can, with very little error, choose the $(2n+l)$ to be the integers which define oscillator levels. In that case when an oscillator shell is just filled (i.e. $N = 2, 8, 20, 40, 70 \ldots$), if K is the largest value of $2n+l$ among the occupied states,

$$N = 1/3\,(K+1)(K+2)(K+3) \tag{36a}$$

and

$$\sum_N{}'\,(2n+l+3/2) = 3/4\,N(K+2). \tag{36b}$$

Then we have, neglecting the spin and orbital terms, from (33), (34), (35), (36)

$$B_N \approx -\tfrac{1}{2}\,V_0 + 3/8(1+\mu^*/2M)(K+2)\hbar\sqrt{(2V_0)}/(a_v A^{1/3}\sqrt{\mu^*}).$$

Now B_N is very nearly constant in all nuclei. Since we see from (36a) that $(K+2)$ varies like $N^{1/3}$, the required constancy of B_N is obtained only if μ^*/M is at least very nearly the same in all nuclei. We choose to define μ^*/M to be the same in all nuclei so that the model potential for neutrons in any nucleus can be specified by three parameters a_r, V_0, and μ^*/M.

The model potential for protons can easily be found by making a suitable allowance for the Coulomb forces. If the charge density be supposed to decrease as the square of the radius within $r < R_r$, then the Coulomb potential there is a quartic in r, taking the values Ze^2/R_r at $r = R_r$ and $1.875Ze^2/R_r$ at $r = 0$. This cavalier treatment can be continued by replacing the quartic by the quadratic form

$$V_c = (1.875-0.875\, r^2/R_r^2)(Ze^2/R_r)$$

which can be added to the neutron potential to form a proton potential with a central depth

$$V_{0P} = V_0 - 1.875Ze^2/R_r \tag{37}$$

and with a level spacing

$$\hbar\omega_P = \hbar\omega_N(1-0.875Ze^2/V_0R_r)^{\frac{1}{2}}. \tag{38}$$

When we have chosen a set of parameters for one nucleus the model described above allows us to extend the choice to all nuclei.

The nucleus Zr^{90} was chosen for initial study. It is large enough for the model concept to be valid but not so large that the matrix elements (31) lose too much accuracy. After some preliminary investigation the matrix of the H.F. Hamiltonian for Zr^{90} was evaluated at $\alpha_N(=\alpha_P) = 0.20$, (.02) to 0.26.

This range of values of α was indicated by nuclear dimensions. From the known relation

$$\int \psi_K^*\, \alpha r^2 \psi_K\, d\tau = (K+3/2)\,,$$

where $K = 2n+l$ is the principal quantum number of the spherical oscillator function ψ_K, we can determine the r.m.s. radius of the nucleons in the oscillator nucleus. For the neutrons of Zr^{90} this ranges from

$$A^{-1/3}\,\langle r^2\rangle^{\frac{1}{2}} = 1.010; \qquad r_0 = 1.304 \text{ at } \alpha = .2$$

$$A^{-1/3}\,\langle r^2\rangle^{\frac{1}{2}} = 0.886; \qquad r_0 = 1.144 \text{ at } \alpha = .26.$$

Here $r_0A^{1/3}$ is the radius of the sphere of uniform density having the given r.m.s. value of radius. The parameter used by Fregeau (1956) to fit Stanford data on electron scattering from O^{16} corresponds for Zr to $\alpha = .210$ although a later fitting (Ehrenberg *et al.* 1959) corresponds to $\alpha = .182$ for Zr.

In general the H.F. matrix elements varied linearly with α, in such wise that the mean binding per neutron varied from -2.90 Mev ($\alpha = 0.20$) to -5.64 Mev ($\alpha = .26$). The element $\langle 04|V|04\rangle$ departs from this behavior to some extent; it decreases more rapidly for $\alpha \gtrsim .22$ than the rest of the

elements, i.e. at the large values of α the almost uniform spacing of diagonal elements (cf. Tables II and III) is slightly disturbed at the highest level, and the total binding energy increases somewhat more rapidly with increasing α.

From an H.F. matrix a "most nearly consistent" model nucleus can be specified. The interval between the $1s$ and $2s$ diagonal elements of the H.F. Hamiltonian is defined to be $2\hbar\omega$. V_0 is then determined from the $1s$ diagonal element. The other model parameters are then also determined, for

$$\mu^*/M = (\hbar^2/M)(\alpha/\hbar\omega)$$

and

$$a_v = (2V_0\mu^*/\hbar^2)^{\frac{1}{2}}/\alpha A^{1/3}.$$

The matrix of the model Hamiltonian can then be compared with the matrix of the H.F. Hamiltonian. This comparison also yielded no definite indication of the best value of α to use, but because of the above-mentioned slightly non-uniform behavior of the $\langle 04|V|04\rangle$ element the spacing of diagonal elements was more nearly uniform at $\alpha = .224$ than at other values of α in the range studied.

The range of values of α is defined approximately by the criterion of nuclear density; within that range the mean binding energy increases with increasing α (decreasing nuclear size) but, otherwise, the results are essentially independent of α. It would have been more satisfactory to determine α by minimizing the energy or by some criterion of consistency. However, such criteria are not satisfied over the reasonable limits of variation of nuclear density; so, lacking any better indication we have decided to use $\alpha = 0.224$ as a basis for a sample computation. The value of the effective mass alters very little (5% from $\alpha = .2$ to $\alpha = .26$) and the "near consistency" of the model does not change significantly. Since these are the points of interest in the calculation the particular value chosen is not important.

The model nucleus from which values of α_N and α_P are drawn is defined by

$$a_v = 1.603 \text{ fermis},$$
$$V_0 = 88.22 \text{ Mev},$$
$$\mu^*/M = 0.6089 \ (M^*/M = 0.7569).$$

SECTION 5. DISCUSSION

The values of $\langle\nu|V|\rho\rangle$ calculated for the parameters (39) are presented in Tables II and III for the four nuclear examples O^{16}, Ca^{40}, Zr^{90}, Ba^{138}. We choose again Zr^{90} as an example for more detailed discussion.

Table II shows the machine output for this case using the potential of (17) including the constants defined there. The complete H.F. Hamiltonian for Zr^{90} is also shown and this matrix for the other nuclei is given in Table III. These matrices contain only the elements between single-particle states which are occupied when the model nucleus is unexcited. The complete solution of the H.F. equations would require the matrix elements between all members of the (complete) set of oscillator functions. Because of the spherical

TABLE II

The non-zero H F. matrix elements for Zr^{90} in Mev. The rows and columns are defined by the quantum numbers (n_ρ, l_ρ) of the radial functions, which are defined by the model parameters $a_v = 1.603$, $V_0 = 88.22$ Mev, $\mu^*/M = .6089$

$n_\nu l_\nu$ $n_\rho l_\rho$	$\langle\nu\|V\|\rho\rangle_{Ex}$	$\langle\nu\|V\|\rho\rangle_D$	$\langle\nu\|V\|\rho\rangle$	$\langle\nu\|T\|\rho\rangle$	$\langle\nu\|H\|\rho\rangle$
Neutrons					
$\langle 00 \mid \mid 00\rangle$	−24.64	−47.66	−72.30	6.97	−65.33
$\langle 01 \mid \mid 01\rangle$	−20.52	−40.54	−61.06	11.62	−49.44
$\langle 02 \mid \mid 02\rangle$	−16.48	−33.98	−50.46	16.26	−34.20
$\langle 10 \mid \mid 10\rangle$	−16.24	−34.83	−51.07	16.26	−34.81
$\langle 03 \mid \mid 03\rangle$	−12.62	−28.03	−40.65	20.91	−19.74
$\langle 11 \mid \mid 11\rangle$	−12.04	−29.56	−41.60	20.91	−20.69
$\langle 04 \mid \mid 04\rangle$	− 8.36	−22.76	−31.12	25.56	− 5.56
$\langle 00 \mid \mid 10\rangle$	− 1.680	− 8.721	−10.401	5.691	− 4.710
$\langle 01 \mid \mid 11\rangle$	− 2.405	−10.368	−12.773	7.347	− 5.426
				Model $\hbar\omega_N$	15.26
Protons					
$\langle 00 \mid \mid 00\rangle$	−27.45	−33.99	−61.44	6.69	−54.75
$\langle 01 \mid \mid 01\rangle$	−23.12	−27.87	−50.99	11.15	−39.84
$\langle 02 \mid \mid 02\rangle$	−18.68	−22.11	−40.79	15.60	−25.19
$\langle 10 \mid \mid 10\rangle$	−18.19	−22.64	−40.83	15.60	−25.23
$\langle 03 \mid \mid 03\rangle$	−14.00	−16.79	−30.79	20.06	−10.73
$\langle 11 \mid \mid 11\rangle$	−12.99	−17.90	−30.89	20.06	−10.83
$\langle 00 \mid \mid 10\rangle$	− 1.723	− 7.490	− 9.213	5.460	− 3.753
$\langle 01 \mid \mid 11\rangle$	− 2.621	− 9.112	−11.733	7.049	− 4.684
				Model $\hbar\omega_P$	14.64

TABLE III

The non-zero elements of the H.F. Hamiltonian matrices, in Mev, for some other systems. The numerical values of the exchange contributions to the elements marked (?) are doubtful due to truncation errors in the machine calculation. The model constants are $a_v = 1.603$, $V_0 = 88.22$ Mev, $\mu^*/M = 0.6089$

	Ba^{138}		Ca^{40}		O^{16}	
	N	P	N	P	N	P
$\langle 00\|H\|00\rangle$	−68.32	−57.38	−56.23	−49.19	−40.25	−37.49
$\langle 01\|H\|01\rangle$	−54.65	−44.25	−36.19	−29.32	−16.46	−13.50
$\langle 02\|H\|02\rangle$	−41.09	−31.20	−17.63	−10.75		
$\langle 10\|H\|10\rangle$	−40.94	−31.14	−19.43	−12.12		
$\langle 03\|H\|03\rangle$	−27.98	−18.68				
$\langle 11\|H\|11\rangle$	−28.71	−18.46				
$\langle 04\|H\|04\rangle$	−13.66(?)	− 2.42(?)				
$\langle 12\|H\|12\rangle$	−16.81	− 6.22				
$\langle 20\|H\|20\rangle$	−16.65					
$\langle 05\|H\|05\rangle$	− 6.66(?)					
$\langle 00\|H\|10\rangle$	− 3.936	− 3.612	− 5.345	− 5.152		
$\langle 00\|H\|20\rangle$	+ 0.280					
$\langle 01\|H\|11\rangle$	− 5.197	− 4.669				
$\langle 02\|H\|12\rangle$	− 5.625	− 5.328				
$\langle 10\|H\|20\rangle$	− 6.106					
Model $\hbar\omega$	13.24	12.58	20.00	19.47	27.15	26.76

symmetry non-zero off-diagonal matrix elements occur only between states having the same l, and therefore separated in energy by $2\hbar\omega$. The samples we have of these off-diagonal elements show them to be small. For example if we diagonalize the truncated Zr matrix for neutrons the eigenvalues differ from the diagonal values by at most 1.00 Mev, and the proper solution $aR_{11}+bR_{01}$, which belongs to the eigenvalue -19.70 (cf. diagonal element -20.69), has $b/a = -0.18$. The interval between the diagonal elements is very nearly constant. Similar results hold for the other Hamiltonian matrices.

These are admittedly only indications of the actual form of the self-consistent solution of the H.F. equations. The effect of including the complete set of states is not known. We can only point out that had all the off-diagonal elements between occupied states been zero there would have been a strong presumption that the original oscillator functions were self-consistent, so that it seems fair to describe the results shown in Tables II and III as nearly consistent. We have not carried the computation any further for obvious reasons, but the presented results suggest that a self-consistent calculation starting from oscillator functions would converge more rapidly than the similar computation for a square well (Rotenberg 1955; Talman 1956).

In none of these calculations does one obtain a good value of the binding energy. The average binding of a neutron and a proton in each of our calculated systems is listed in Table IV and these are all clearly too small in magni-

TABLE IV

Binding energies per nucleon and the mean neutron one-body potential from H.F. calculation

	$\bar{B}_N$, Mev	$\bar{B}_P$, Mev	$\bar{V}_N$, Mev
O^{16}	-1.908	-0.583	41.00
Ca^{40}	-4.470	-1.680	45.48
Zr^{90}	-3.424	-2.468	44.95
Ba^{138}	-2.835	-2.472	44.30

tude. We cannot expect to obtain correct binding energies in a calculation which ignores correlations of motions of nucleons in a nucleus (Jastrow 1955; Aviles 1958), and to deal with those an internucleon potential which describes interactions at high energy is required. However, the present computation was made to examine the relative usefulness of the oscillator wave functions for the initial unperturbed shell model functions, not in the expectation of properly computing the nuclear binding energy.

On the other hand, the spacing of single-particle levels is quite reasonable, and this is perhaps more significant for our purpose. Tables II and III show the single-particle model value of $\hbar\omega$. Comparison with the diagonal H.F. matrix elements shows that this is reproduced within small error except near the top of the system of levels.

Moreover the value of $\hbar\omega$ derived here is nearly consistent with observations on physical nuclei. It has been found (Newton 1956) that the observed level spacings in nuclei can be fitted by assuming that the spacing between j-shells of one type of nucleon is uniform and has, at the top of the occupied set, the value $(0188A^{2/3})^{-1}$ Mev. Since there are $K+1$ j-shells in the Kth oscillator shell, this yields

$$\hbar\omega_N \approx 53.0(K+1)A^{-2/3} \text{ Mev.}$$

When the system contains closed oscillator shells the largest value of K is related to the neutron number N by (36a) so that $(K+1)\sim(3N)^{1/3}\sim(3/2A)^{1/3}$. Thus from the level-spacing study one obtains the approximation

$$\hbar\omega_N \approx 65A^{-1/3}. \tag{40}$$

The set (39) of parameters for the cutoff oscillator model yield

$$\begin{aligned}\hbar\omega_N &= 2a_v^{-1}(\hbar^2/2M)^{1/2}\sqrt{V_0M/\mu^*}A^{-1/3} \\ &= 68A^{-1/3}.\end{aligned} \tag{41}$$

The "almost consistent" model nucleus thus has spacings very similar to those deduced from the spacings of nuclear levels. This is a better result than the calculated binding energy. However, it must be pointed out that equation (40) is derived from the single-particle level density at the top of the occupied set of levels while it has been observed that the H.F. levels are more closely spaced at the top.

The H.F. study has been confined to states occupied when the model nucleus is unexcited. The degree of consistency exhibited by the oscillator functions therefore is demonstrated only in the region of space in which the ground state particle density is appreciably different from zero. In order to conclude that the equivalent one-body potential is approximately quadratic in r from $r = 0$ to the nuclear boundary we require the results of Section 2, which show that the oscillator functions are nearly exact solutions of a potential which is quadratic in r for $r \leqslant R_v$ and zero outside the nuclear surface.

It is obvious that this calculation leads to no very definite conclusion. We have only shown an indication that the oscillator single-particle wave functions are close to the self-consistent solution for the potential (17). However, this statement, such as it is, holds for all the systems investigated. So far as the evaluation of $\langle\rho|V|\nu\rangle$ is concerned, the significant measure of the range of the internucleon potential is $\sqrt{\alpha}/\mu$, where μ is the Yukawa constant (equation 17) and $\alpha = (\mu^*\omega)/\hbar$. Since $\alpha \sim A^{-1/3}$, the "near consistency" is not very sensitive to the range of the internucleon force. This was also demonstrated by the initial calculations for Zr^{90} at various $\alpha_N = \alpha_P$. In like fashion a change of the strength $\frac{1}{2}Ce^2$ of potential (17) will simply change $\langle\rho|V|\nu\rangle$ proportionately. This will not change the regularity of the interval between diagonal elements, though it will change the relative value of the off-diagonal elements. Thus the "near consistency" is not very sensitive to the strength of the potential (17). In this connection one can note that it would require a 25% increase of the strength constant C to bring the mean binding energies into qualitative agreement with measurement.

The parameters (39) were derived in a quite arbitrary fashion. It would clearly be possible by slightly increasing V_0 and a_v to retain for the model a value of $\hbar\omega$ close to (40) and a reasonable value (8.5 Mev) for the binding energy per neutron. This might be supposed to represent the results of a better variational procedure.

It is easily seen from equation (35) that if the model yields a qualitatively reasonable value for the mean binding it will yield also a reasonable value of the separation energy of the last particle, i.e. the energy required to remove a neutron is

$$S_N = NB_N^{(A)} - (N-1)B_N^{(A-1)},$$

so that

$$(42) \quad S_N - B_N = \{N-1-N(1-A^{-1})^{-1/3}\}(1/2V_0+B_N)+(1-A^{-1})^{-1/3}T_N$$

in which B_N is defined by (35) and T_N is the last summand on the right side of (35). The superscripts on B_N denote the nucleus in which the mean binding is computed. V_0 is assumed to be independent of the nucleus and B_N is known to be nearly so. The difference (42) increases more or less uniformly and slowly with A, if N be chosen on the line of nuclear stability. When $C = D = 0$ the change in (42) is about 2.5 Mev from oxygen to lead, and this variation is significantly increased when C and D are Nilsson's (1955) values. The direction and order of magnitude of this variation agree with observation.

We thus conclude that a shell model based on the cutoff oscillator well could be defined so as to yield a reasonable account of the binding energies as well as to exhibit the other well-known resemblances to physical nuclei. However, it is not possible uniquely to define the parameters of the well by these requirements. This definition should be made by a method based on known internucleon interactions. The partial success of the present simple calculation allows hope that this can be done.

ACKNOWLEDGMENTS

The writer is grateful to Dr. Erich Vogt for time taken in several useful discussions. The calculations reported in this paper were performed on the Chalk River datatron, making use where possible of library routines prepared under the direction of Dr. J. M. Kennedy. The calculations described in Section 2 were programed by Mr. D. Kuehner.

REFERENCES

AVILES, J. B. 1958. Ann. Phys. **5**, 251.
BATEMAN MANUSCRIPT PROJECT. 1953. Higher transcendental functions (McGraw Hill Book Co., Inc.)
BETHE, H. A. 1956. Phys. Rev. **103**, 1353.
BLATT, J. M. and WEISSKOPF, V. F. 1952. Theoretical nuclear physics (John Wiley & Sons, Inc., New York).
BOHR, A. and MOTTELSON, B. R. 1953. Kgl. Danske Videnskab. Selskab, Mat.-fys. Medd. **27**, No. 16.
BRUECKNER, K. A. 1959. Proceedings of the Tallahassee Conference on Optical Model, University of Florida.
BRUECKNER, K. A. and GAMMEL, J. L. 1958. Phys. Rev. **109**, 1023.
EHRENBERG, H. F., HOFSTADTER, R., MEYER-BERKHOUT, U., RAVENHALL, D. G., and SOBOTTKA, E. E. 1959. Phys. Rev. **113**, 666.
ELLIOTT, J. P. 1958. Proc. Roy. Soc. A, **245**, 562.
FESHBACH, H. and SCHWINGER, J. 1951. Phys. Rev. **84**, 194.
FREGEAU, J. H. 1956. Phys. Rev. **104**, 225.
GAMMEL, J. L. and THALER, R. M. 1957. Phys. Rev. **107**, 291, 1337.
GOMES, L. C., WALECKA, J. D., AND WEISSKOPF, V. F. 1958. Ann. Phys. **3**, 241.
HALL, H. H. and POWELL, J. L. 1953. Phys. Rev. **90**, 912.

HAXEL, O., JENSEN, J. H. D., and SUESS, H. E. 1949. Phys. Rev. **75**, 1766.
——— 1949. Naturwissenshaften, **36**, 153.
HUANG, K. and YANG, C. N. 1957. Phys. Rev. **105**, 767.
JASTROW, R. 1955. Phys. Rev. **98**, 1479.
LANE, A. M., THOMAS, R. G., and WIGNER, E. P. 1955. Phys. Rev. **98**, 693.
LEE, T. D., HUANG, K., and YANG, C. N. 1957. Phys. Rev. **106**, 1135.
LITHERLAND, A. E., PAUL, E. B., BARTHOLOMEW, G. A., and GOVE, H. E. 1956. Phys. Rev. **102**, 208.
MAYER, M. G. 1949. Phys. Rev. **75**, 1969.
MOTT, M. and SNEDDON, I. N. 1948. Wave mechanics and its applications (Oxford University Press).
MOTTELSON, B. R. and NILSSON, S. G. 1955. Phys. Rev. **99**, 1615.
NEWTON, T. D. 1956. Can. J. Phys. **34**, 804.
NILSSON, S. G. 1955. Kgl. Danske Videnskab. Selskab, Mat.-fys. Medd. **29**, No. 16.
ROTENBERG, R. 1955. Phys. Rev. **100**, 439.
SIGNELL, P. S. and MARSHAK, R. E. 1958. Phys. Rev. **109**, 1229.
TALMAN, J. D. 1956. Phys. Rev. **102**, 455.
TALMI, I. 1952. Helv. Phys. Acta, **25**, 185.
TAUBER, G. E. and WU, T. Y. 1957. Phys. Rev. **105**, 1772.
WATSON, G. N. 1952. Theory of Bessel functions. 2nd ed. (Cambridge University Press, London).

APPENDIX

To illustrate the concept of pseudo-potential used in Section 4 consider the potential consisting of a square attractive well with a repulsive core;

$$\text{(A1)} \qquad \begin{aligned} V &= +\infty && 0 \leqslant r \leqslant r_0 \\ &= -V_0 && r_0 < r \leqslant r_1 \\ &= 0 && r_1 < r. \end{aligned}$$

The corresponding pseudo potential will be constructed as a momentum-dependent square well with no repulsive core. For a specified angular momentum l between the fragments we assume

$$\text{(A2)} \qquad \begin{aligned} V^*(l, E) &= -V_0^*(l) + V(E, l) && 0 \leqslant r \leqslant r_1 \\ &= 0 && r_1 < r. \end{aligned}$$

The solutions of the Schrödinger equations with potentials (A1) and (A2) are then compared at the boundary surface $r = r_1$. V_0^* is so chosen that the radial logarithmic derivatives of the solutions at this surface have the same value when $E = 0$, and the function $V(E, l)$ is defined so that these remain equal at each positive value of E. One sees the momentum dependence in the fact that the pseudo potential (A2) varies with angular momentum and energy. Now one can suppose that $V^*(E, l)$ may be expanded as a power series in E. To first order in E it may be written as ($k^2 = \hbar^{-2}ME$)

$$\text{(A3)} \qquad V^*(l, E) = -V_0^*(l) + \frac{\hbar^2}{M}\left(1 - \frac{M^*}{M}\right)k^2.$$

Here M^* is an "effective mass". Equation (A3) may be rendered exact by permitting M^* to be itself a function of E. Then the determination of $V_0^*(l)$ and M_l^* reduces to the solution of the transcendental equations

$$\text{(A4)} \qquad \begin{aligned} x^* j_l^{-1}(x^*)\, j_{l-1}(x^*) &= x z_l^{-1}(x)\, z_{l-1}(x) \\ x^* &= r_1 \hbar^{-1} \sqrt{\{M V_0^*(l) + M^* E\}} \\ x &= r_1 \hbar^{-1} \sqrt{\{M(V_0 + E)\}}; \end{aligned}$$

j_l is the spherical Bessel function and z_l the combination of spherical Hankel functions which vanishes at $r = r_0$ and satisfies the Schrödinger equation containing the potential (A1).

The depths $V_0^*(l)$ and effective masses $M^*(l)$ are listed in Table V as functions of energy. The case computed is $V_0 = 184.8$ Mev; $r_0 = 0.4$ fermi

TABLE V

Pseudo potentials of form (A2) with V^* and M^*/M as shown match the potential (A1)

$E = 0$	$V_0^*(0) = 87.39$	$V^*(1) = 152.6$	$V_0^*(2) = 177.5$	$V_0^*(3) = 183.4$	$V_0^*(4) = 184.6$
E, Mev	$M^*(0)/M$	$M^*(1)/M$	$M^*(2)/M$	$M^*(3)/M$	$M^*(4)/M$
5	.638	.886	.977	.997	1.000
20	.637	.885	.977	.997	1.000
40	.633	.884	.977	.997	1.000
60	.629	.882	.977	.997	1.000
80	.623	.880	.976	.997	1.000
100	.617	.878	.976	.997	1.000
120	.609	.875	.975	$.996_5$	1.000
140	.601	.872	$.974_5$	.996	1.000
160	.593	.868	.974	.996	1.000
180	.585	.865	.973	.996	1.000

NOTE: $V = \infty$, $r < 0.4$ fermi; $V = -184.8$ Mev, 0.4 fermi $< r < 1.2$ fermis; $V = 0$, $r > 1.2$ fermis.

and $r_1 = 1.2$ fermis. It is obvious that only the s and p waves are affected by the central core and that a constant effective mass for each angular momentum is a good approximation for energies up to 150 Mev. The d, and higher l, partial waves are affected very little by the core; they are scattered mainly by the potential step at r_1. Consequently the effective mass is very nearly equal to the true mass, and the step in the pseudo potential is very nearly equal to that of the potential (A1) being matched.

ON AN ASYMPTOTIC EXPANSION OCCURRING IN THE EVALUATION OF A LATTICE SUM*

G. H. WEISS† AND A. A. MARADUDIN‡

Recently (Maradudin and Weiss 1959) we have published a method for evaluating lattice sums and, in particular, we have applied it to sums of the form

$$T_s = \sum_{m,n=1}^{\infty} \frac{mn}{(m^2+n^2)^{s/2}}. \tag{1}$$

One of the crucial steps in the method as applied to this problem consists of finding a small t expansion for the function

$$F(t) = \sum_{n=0}^{\infty} n\, e^{-n^2 t}. \tag{2}$$

We used a Poisson summation formula which required us to deal with asymptotic properties of hypergeometric functions. An alternative method which is slightly simpler, and which can be used even when the Fourier transform appearing in the Poisson summation formula cannot be evaluated exactly, is to use the Euler summation formula (Knopp 1951) for this problem. Thus we find

$$\begin{aligned} F(t) &\sim \int_0^{\infty} xe^{-x^2 t}\,dx - \sum_{k=1}^{\infty} \frac{B_{2k}}{(2k)!} \frac{d^{2k-1}}{dx^{2k-1}} (xe^{-x^2 t})_{x=0} \\ &= \frac{1}{2t} - \sum_{k=1} \frac{B_{2k}}{(2k)!} \frac{d^{2k-1}}{dx^{2k-1}} (xe^{-x^2 t})_{x=0}. \end{aligned} \tag{3}$$

But we can also write

$$xe^{-x^2 t} = -\frac{1}{2t} \frac{d}{dx} (e^{-x^2 t}). \tag{4}$$

Hence

$$F(t) \sim \frac{1}{2t} + \frac{1}{2t} \sum_{k=1} \frac{B_{2k}}{(2k)!} \frac{d^{2k}}{dx^{2k}} (e^{-x^2 t})_{x=0}. \tag{5}$$

The derivative terms can be evaluated by changing to a new variable $y^2 = x^2 t$, which implies that $(d/dx) = \sqrt{t}\ (d/dy)$. This yields

*This research was supported by the United States Air Force through the Air Force Office of Scientific Research, Air Research and Development Command under Contract No. AF 18(600)1315.

†Department of Applied Mathematics, Weizmann Institute of Science, Rehovot, Israel.

‡Institute for Fluid Dynamics and Applied Mathematics, University of Maryland, College Park, Maryland.

$$F(t) \sim \frac{1}{2t}+\frac{1}{2t}\sum_{k=1}\frac{B_{2k}}{(2k)!}\,t^k\,\frac{d^{2k}}{dy^{2k}}\,(e^{-y^2})_{y=0}. \tag{6}$$

But it is known (Erdelyi *et al.* 1953) that

$$H_{2n}(y) = e^{y^2}\left(\frac{d}{dy}\right)^{2n}(e^{-y^2}) \tag{7}$$

and

$$H_{2k}(0) = (-1)^k\,\frac{(2k)!}{k!}$$

where $H_n(y)$ is the nth degree Hermite polynomial.
Hence

$$F(t) \sim \frac{1}{2t}-\frac{1}{2t}\sum_{k=1}^{\infty}(-1)^{k-1}\,\frac{B_{2k}}{k!}\,t^k \tag{8}$$

as given.

An alternative, equivalent, derivation of this result proceeds from the representation of $F(t)$ obtained with the aid of the Poisson summation formula (ref. 4, eq. (10)):

$$\begin{aligned} F(t) &= \frac{1}{2}\sum_{n=-\infty}^{\infty}\int_{-\infty}^{\infty}|x|\,e^{-x^2t}\cos 2\pi\,nx\,dx \\ &= \frac{1}{2t}+2\sum_{n=1}\int_0^{\infty}xe^{-x^2t}\cos 2\pi\,nx\,dx. \end{aligned} \tag{9}$$

It is proved by Lighthill (1958) that if $F(x)$ and all its derivatives exist as ordinary functions for $x \geqslant 0$ and are well behaved at infinity, then

$$\int_0^{\infty}F(x)\cos 2\pi\,x\,y\,dx \sim \sum_{m=1}(-1)^m\,\frac{F^{(2m-1)}(0)}{(2\pi y)^{2m}} \tag{10}$$

as $y \to \infty$. With this result eq. (9) becomes

$$\begin{aligned} F(t) &\sim \frac{1}{2t}+2\sum_{m=1}\frac{(-1)^m}{(2\pi)^{2m}}\,\frac{d^{2m-1}}{dx^{2m-1}}\,(xe^{-x^2t})_{x=0}\sum_{n=1}^{\infty}\frac{1}{n^{2m}} \\ &= \frac{1}{2t}-\sum_{m=1}^{\infty}\frac{B_{2m}}{(2m)!}\,\frac{d^{2m-1}}{dx^{2m-1}}\,(xe^{-x^2t})_{x=0} \end{aligned}$$

which is just eq. (3).

ERDELYI, A., MAGNUS, W., and OBERHETTINGER, F. 1953. Higher transcendental functions, Vol. 2 (McGraw-Hill Book Co., Inc., New York), p. 193.
KNOPP, K. 1951. Theory and application of infinite series (Blackie and Son Ltd., London), p. 518.
LIGHTHILL, M. J. 1958. An introduction to Fourier analysis and generalized functions (Cambridge University Press, Cambridge), p. 56.
MARADUDIN, A. A. and WEISS, G. H. 1959. Can. J. Phys. **37**, 170.

RECEIVED MAY 4, 1959.
INSTITUTE OF FLUID DYNAMICS AND APPLIED MATHEMATICS,
UNIVERSITY OF MARYLAND,
COLLEGE PARK, MARYLAND.

NOTES TO CONTRIBUTORS

Canadian Journal of Physics

MANUSCRIPTS

General.—Manuscripts, in English or French, should be typewritten, double spaced, on paper 8½×11 in. **The original and one copy are to be submitted.** Tables and captions for the figures should be placed at the end of the manuscript. Every sheet of the manuscript should be numbered. Style, arrangement, spelling, and abbreviations should conform to the usage of recent numbers of this journal. Greek letters or unusual signs should be written plainly or explained by marginal notes. Characters to be set in boldface type should be indicated by a wavy line below each character. Superscripts and subscripts must be legible and carefully placed. Manuscripts and illustrations should be carefully checked before they are submitted. Authors will be charged for unnecessary deviations from the usual format and for changes made in the proof that are considered excessive or unnecessary.

Abstract.—An abstract of not more than about 200 words, indicating the scope of the work and the principal findings, is required, except in Notes.

References.—References should be listed **alphabetically by authors' names,** unnumbered, and typed after the text. The form of the citations should be that used in current issues of this journal; in references to papers in periodicals, titles should not be given and only initial page numbers are required. The names of periodicals should be abbreviated in the form given in the most recent *List of Periodicals Abstracted by Chemical Abstracts.* All citations should be checked with the original articles and each one referred to in the text by the authors' names and the year.

Tables.—Tables should be numbered in roman numerals and each table referred to in the text. Titles should always be given but should be brief; column headings should be brief and descriptive matter in the tables confined to a minimum. Vertical rules should not be used. Numerous small tables should be avoided.

ILLUSTRATIONS

General.—All figures (including each figure of the plates) should be numbered consecutively from 1 up, in arabic numerals, and each figure referred to in the text. The author's name, title of the paper, and figure number should be written in the lower left corner of the sheets on which the illustrations appear. Captions should not be written on the illustrations.

Line drawings.—Drawings should be carefully made with India ink on white drawing paper, blue tracing linen, or co-ordinate paper ruled in blue only; any co-ordinate lines that are to appear in the reproduction should be ruled in black ink. Paper ruled in green, yellow, or red should not be used. All lines must be of sufficient thickness to reproduce well. Decimal points, periods, and stippled dots must be solid black circles large enough to be reduced if necessary. Letters and numerals should be neatly made, preferably with a stencil (**do NOT use typewriting**) and be of such size that the smallest lettering will be not less than 1 mm high when the figure is reduced to a suitable size. Many drawings are made too large; originals should not be more than 2 or 3 times the size of the desired reproduction. Whenever possible two or more drawings should be grouped to reduce the number of cuts required. In such groups of drawings, or in large drawings, full use of the space available should be made; the ratio of height to width should conform to that of a journal page (4¾×7½ in.), but allowance must be made for the captions. **The original drawings and one set of clear copies (e.g. small photographs) are to be submitted.**

Photographs.—Prints should be made on glossy paper, with strong contrasts. They should be trimmed so that essential features only are shown and mounted carefully, with rubber cement, on white cardboard, with no space between those arranged in groups. In mounting, full use of the space available should be made. **Photographs are to be submitted in duplicate;** if they are to be reproduced in groups one set should be mounted, the duplicate set unmounted.

REPRINTS

A total of 50 reprints of each paper, without covers, are supplied free. Additional reprints, with or without covers, may be purchased at the time of publication.

Charges for reprints are based on the number of printed pages, which may be calculated approximately by multiplying by 0.6 the number of manuscript pages (double-spaced typewritten sheets, 8½×11 in.) and including the space occupied by illustrations. Prices and instructions for ordering reprints are sent out with the galley proof.

Contents

Printed in Canada *by* University of Toronto Press